scientific reports

OPEN

Antisense mediated blockade of Dickkopf 1 attenuates tumor survival, metastases and bone damage in experimental osteosarcoma

Andrew Haskell[1,4], Simin Pan[1,4], Robert Reese[2], Anthony Powers[2], Megan G. Lopez[1], Sebastian Lomeli[1], Christopher Story[1], Joshua Benton[1], J. Chris Blazier[3], Roland Kaunas[1,2] & Carl A. Gregory [ID][1]✉

Osteosarcoma (OS) is the most common primary bone malignancy. The canonical Wnt inhibitor Dickkopf-1 (Dkk-1) has been implicated in bone destruction, tumor survival and metastases during OS. We examined the role of Dkk-1 in OS disease progression and explored strategies for targeting its activity. Dkk-1 enhances OS survival by amplifying a non-canonical Wnt pathway that upregulates aldehyde dehydrogenase 1A1. Targeting of Dkk-1 transcription with a vivo morpholino (DkkMo) reduced OS survival and enhanced osteogenic activity of OS in vitro. DkkMo as a single agent slowed tumor expansion, increased tumor necrosis, inhibited metastases and preserved bone in a PDX model of OS. DkkMo also reduced the frequency of dividing tumor cells and reinitiated a regenerative osteogenic phenotype in tumors and stroma while reducing infiltration of inflammatory cells. These findings indicate that DkkMo has the potential to safely target osteosarcoma growth, survival, metastases and bone destruction.

Keywords Osteosarcoma, Dickkopf-1, Wnt, Antisense morpholino

Osteosarcoma (OS) is the most common primary bone malignancy accounting for 9% of pediatric cancer deaths[1]. The incidence rate of OS is estimated to be 8–11 million per year between the ages of 15–19 and with a second peak in individuals over 60 years[2]. Common strategies for treating OS involves tumor ablation or amputation accompanied by chemotherapy[3]. Chemotherapy increases 5 year event-free survival (EVS) from 20–40% (surgery alone) to 50–90%[4]. Nevertheless, the probability of 5-year EVS is substantially reduced if patients present with metastases[2]. With overall variable 5-year EVS rates for OS between 36 and 86% over recent years[2,5,6], there is a need for more potent treatment strategies.

OS tumors secrete the 35 kDa extracellular ligand Dickkopf-Wnt-signaling-pathway-inhibitor-1 (Dkk-1) with the capacity to inhibit canonical Wnt (cWnt) signaling which drives the differentiation of mesenchymal stem cells (MSCs) to osteoblasts[7]. Dkk-1-mediated dysregulation of bone turnover causes catastrophic bone damage[8,9] and has the capacity to reprogram adjacent MSCs into tumor-supporting cells[10,11], thereby providing a protective niche for tumor propagation[12] and increasing the potential for drug resistant cell selection and refractory disease[10,12–16]. Dkk-1 also activates tumor survival pathways mediated by non-canonical Wnt signaling (ncWnt)-triggered Jun kinase (JNK) activity[9,17,18] that in turn stimulates expression of stress response factors such as aldehyde dehydrogenase 1A1 (ALDH1A1)[9]. ALDH1A1 neutralizes chemical stressors arising from chemotherapy, nutritional stress, and rapid proliferation[19,20], and it is also a biomarker for the tumor initiator phenotype and metastatic potential[21–26].

We recently demonstrated that an antisense phosphorodiamidate morpholino oligomer conjugated to a cell-penetrating octa-guanidine dendrimer (also referred to as a *vivo* morpholino), blocks Dkk-1 output and reduces bone destruction in a murine model of OS typically characterized by high and constitutive levels of

[1]Department of Medical Physiology, Texas A&M College of Medicine, Bryan, TX 77807, USA. [2]Department of Biomedical Engineering, Texas A&M University, Emerging Technologies Building, College Station, TX, USA. [3]Texas A&M Institute for Genome Sciences and Society, College Station, TX, USA. [4]Andrew Haskell and Simin Pan contributed equally to this work. ✉email: cgregory@tamu.edu
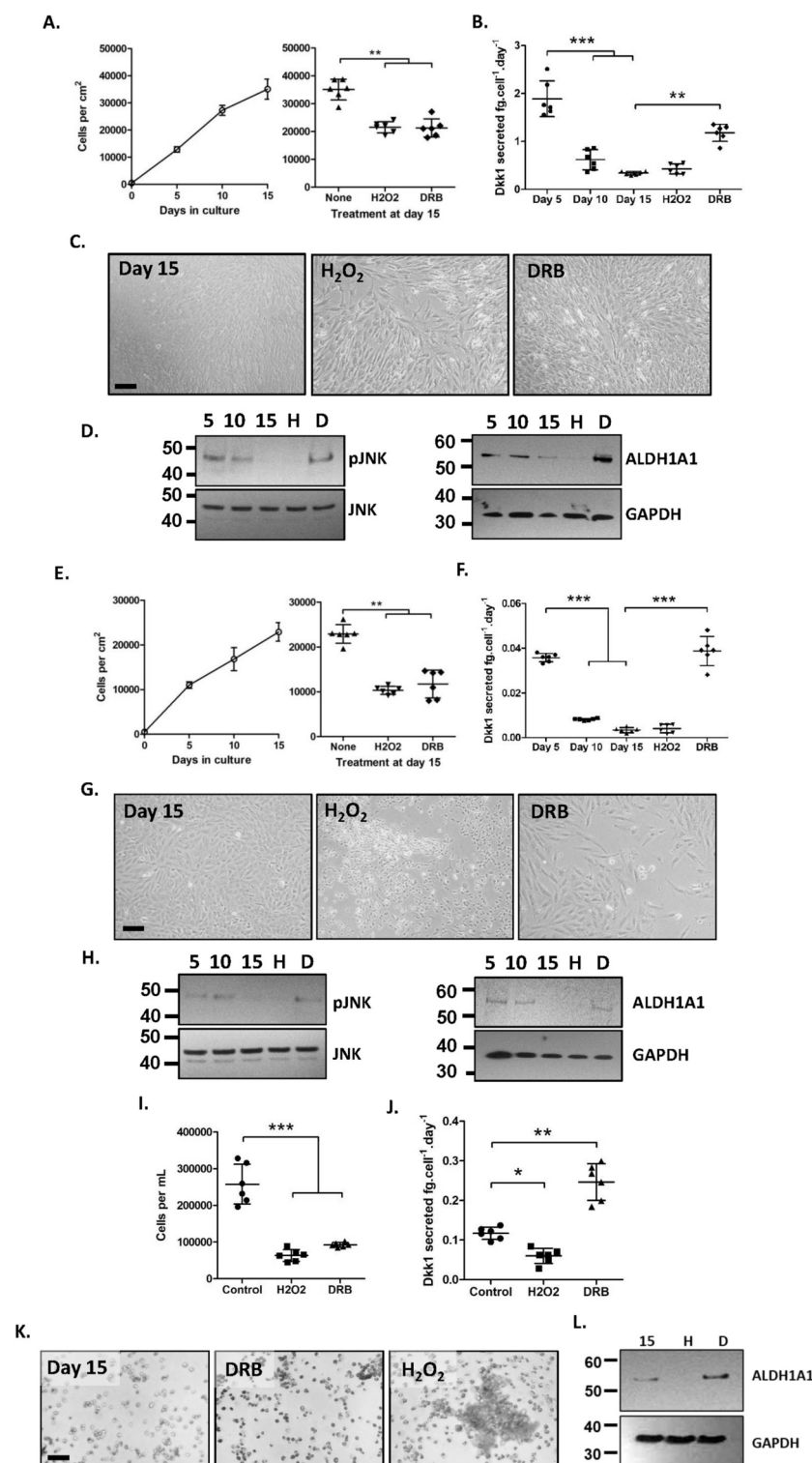
Dkk-1[27]. As a single agent and when co-administered with DRB, the vivo morpholino, referred to hereafter as *DkkMo*, significantly increased the volume and number of necrotic lesions in the tumor and reduced the rate of tumor growth[27]. Herein, we expand studies to human OS cell lines and a patient derived OS xenograft (PDX-OS), hypothesizing that DkkMo has the capacity to perturb OS survival, reduce bone destruction, and inhibit metastasis of experimental OS tumors in part through a mechanism involving ncWnt, JNK, and ALDH1A1.

Results

Proliferative and chemical stress responses correlate with upregulation of Dkk1 and ALDH1A1

In MSCs and cultured OS cells, Dkk-1 output has been reported to peak during high rates of proliferation[28,29]. To gain insight into how proliferative activity affects Dkk-1 and ALDH1A1 output, human OS cell lines (MG63 and

◄**Fig. 1**. Proliferation and chemotherapeutic stress correlates with upregulation of Dkk1 and ALDH1A1 expression and JNK phosphorylation by human OS and MM cell lines. (**A,E**) Growth curves of MG63 (panel A, left) and SAOS (panel E, left) human OS cell lines under standard conditions. At day 13, some cultures were treated with DRB or H_2O_2 and assayed at day 15 (panel A and E, right). (**B,F**) ELISA assays of Dkk-1 in media supernatants of MG63 (panel B) and SAOS (panel F) cultures. (**C,G**) Phase-contrast micrographs of MG63 (panel C) and SAOS (panel G) cultures at day 15 (bar = 100 μm). (**D,H**) Immunoblots of MG63 (panel D) and SAOS (panel H) cells for phosphorylated JNK (*left*) and ALDH1A1 (*right*) at day 5, 10 and 15 and at day 15 with DRB (D) or H_2O_2 (H). (**I**) Yields of INA6 MM cells after 15 days of standard culture or treatment at day 13 with H_2O_2 or DRB. (**J**) ELISA assays of Dkk-1 in media supernatants after 15 days under conditions in panel I. (**K**) Phase contrast micrographs of INA6 cultures under conditions in panel I at day 15 (bar = 100 μm). (**L**) Immunoblots of INA6 cells for ALDH1A1 under conditions in panel I. Statistics: ANOVA and Tukey's multiple comparison test. *p<0.05, **p < 0.01, ***p < 0.005, n = 6.

SAOS) were seeded at low density and allowed to proliferate to confluency. Cells were counted (Fig. 1A, E) and Dkk-1 secretion (Fig. 1B, F) was measured. MG63 cells secreted 50 times more Dkk-1 (Fig. 1B) than SAOS cells (Fig. 1F), but in both cases, Dkk-1 output was maximal when measured during the rapid phase of proliferation (day 5) and reduced by 6- to tenfold at confluency (day 15).

To examine whether chemical stresses could trigger Dkk-1 output, healthy confluent monolayers at day 13 were exposed to H_2O_2 to immediately introduce reactive oxygen species (ROS), or doxorubicin (DRB) which has a more gradual effect on DNA integrity and ROS accumulation[30]. These experiments were performed only on established cultures because performing growth curves in the presence of DRB and H_2O_2 was challenging to reproduce with sufficient numbers of cultured cells for analysis. This is likely attributable to the stochastic effects of DRB and H_2O_2 and the relatively low starting density of the cultures. After 2 days, H_2O_2 caused morphological signs of cell destruction especially in SAOS cells (Fig. 1C, G), and reduced cell numbers (Fig. 1A, E) but failed to significantly upregulate Dkk-1 (Fig. 1B, F). DRB treatment also caused a reduction in cell number (Fig. 1A, E), but signs of cell damage were reduced (Fig. 1C, G). DRB treatment elevated Dkk-1 expression in stationary confluent monolayers to a degree that was comparable to rapidly dividing cultures (Fig. 1B, F).

Dkk-1 has the capacity to upregulate JNK in a murine OS cell line which in turn upregulates ALDH1A1 expression and resistance to chemical and nutritional stressors[9]. In both SAOS and MG63 cells, JNK phosphorylation and ALDH1A1 expression correlated with Dkk-1 expression in proliferative cells and with DRB treatment (Fig. 1D, H). In the non-adherent MM cell line INA6, Dkk-1 and ALDH1A1 expression was also upregulated in response to DRB, but not H_2O_2 (Fig. 1I–L).

Collectively, these data indicate a correlation between proliferation, Dkk-1 output, and the activity of JNK and ALDH1A1, suggesting that proliferative stress is one trigger for a Dkk-1 mediated stress response. Dkk-1, JNK, and ALDH1A1 were also upregulated with DRB treatment, but not H_2O_2, suggesting that ROS alone are not necessarily sufficient to upregulate Dkk-1.

### Dkk1 promotes ALDH1A1 expression via the PCP-like ncWnt/JNK signaling axis

To establish whether there was a functional relationship between Dkk-1 and resistance to introduction of stress, expression of Dkk-1 was depleted in MG63 cells by a constitutively expressed Dkk-1-specific shRNA (MG63-kdDkk1) and compared to control MG63 cells with a scrambled shRNA (MG63-scr). MG63-kdDkk1 cells exhibited substantial reductions in Dkk-1 secretion (Fig. 2A) and transcription (Fig. 2B) when assayed at the same cell density (Fig. 2C). MG63-kdDkk1 cells accumulated slower than MG63-scr cells, especially at higher densities (Fig. 2D), and exhibited reduced capacity to survive nutritional stress caused by medium deprivation (replenishment of 25% of the medium) (Fig. 2E). MG63-kdDkk1 cells were also more susceptible to DRB than controls (Fig. 2F). These data indicate that deprivation of Dkk-1 results in attenuated survival potential when challenged by proliferative, nutritional and chemical stressors in MG63 cells.

We previously reported that constitutive expression of Dkk-1 inhibits cWnt, shifting the balance in favor of a polar cell polarity (PCP)-like ncWnt pathway that results in activation of JNK through activation of RhoA and mitogen-activated-protein-kinase-kinase-4 (MAPKK4). Enhanced JNK activity in turn stimulates Jun transcription factor to upregulate expression of protective enzymes such as ALDH1A1[9]. In comparison to MG63-scr controls, MG63-kdDkk1 cells exhibited a reduction in total RhoA protein, reduction in the phosphorylation status of MKK4 and JNK (Fig. 2G), and significantly depleted levels of ALDH1A1 that was further confirmed by densitometric measurements of replicate samples (Fig. 2H). Together, these data indicate that Dkk-1 signals through a RhoA/Mkk4/JNK mediated axis to activate expression of ALDH1A1.

With osteogenic stimulus, MG63-kdDkk1 cells secreted higher levels of osteogenic biomarkers osteoprotegerin (OPG) (Fig. 2I), alkaline phosphatase (ALP) (Fig. 2J), and exhibited a faster rate of biomineralization as assayed by alizarin red S staining (Fig. 2K, L). These data support the general understanding that Dkk-1 inhibits cWnt which drives early stages of osteogenic differentiation[31–34] and provide credence to the potential role of Dkk-1 in contributing to the dedifferentiated status of highly aggressive forms of OS.

Targeting components of the PCP-like ncWnt pathway with inhibitors

To identify potential means to perturb the PCP-like ncWnt pathway, several inhibitors targeting different components of the PCP-like ncWnt and cWnt pathways were incubated with MOSJ-Dkk1 cells. MOSJ cells expressing constitutive Dkk-1 (MOSJ-Dkk1 cells) were used for these experiments because Dkk-1 output is resistant to fluctuations caused by proliferative status or stress responses[9,27]. This was confirmed experimentally through exposure of confluent cultures of MOSJ-Dkk1 cells and their control counterparts (MOSJ-scr) to 10^{-8} mM
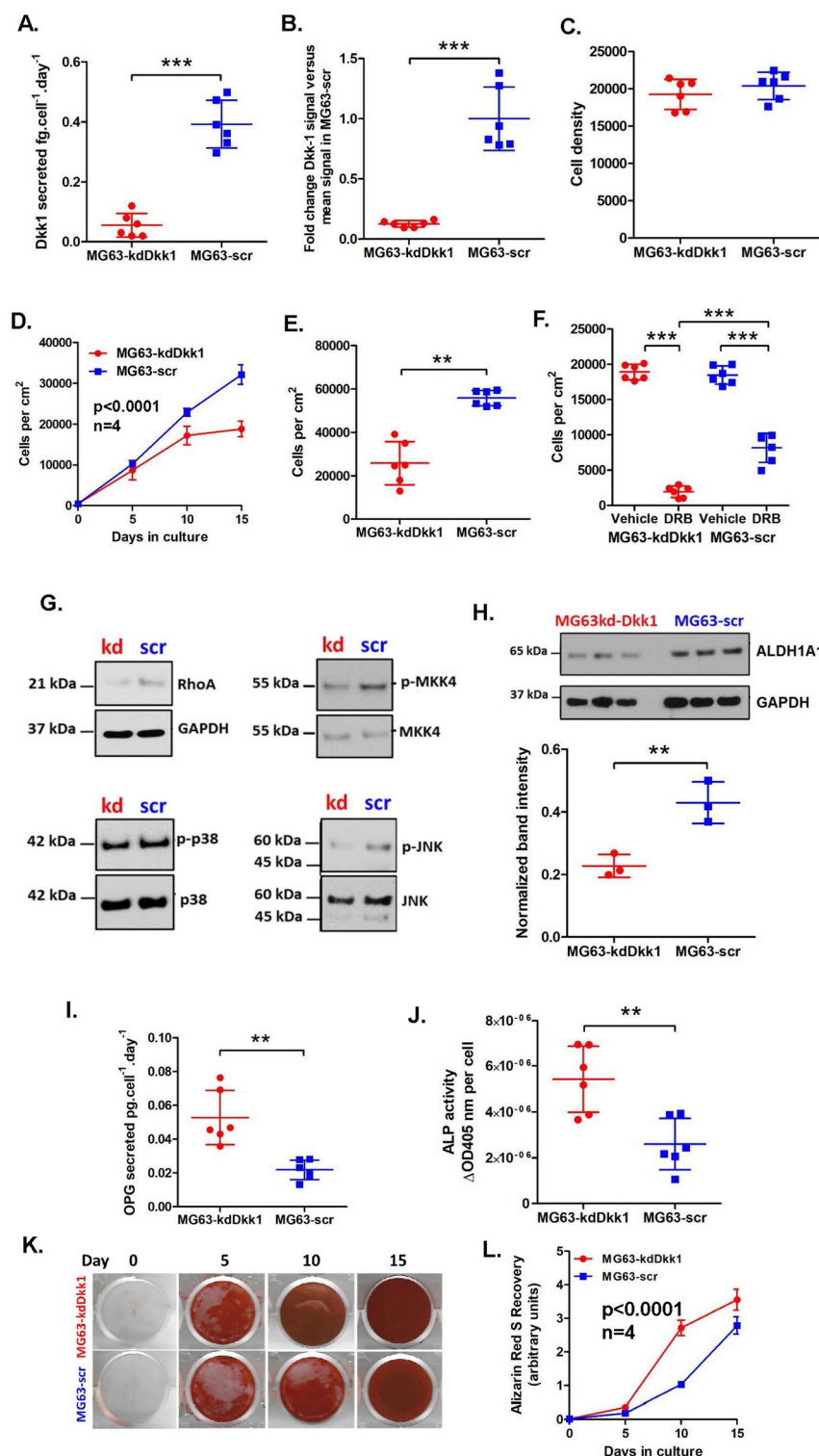
doxorubicin and nutritional deprivation (Fig. 3A). MOSJ-Dkk1 cells were exposed to multiple concentrations of specific inhibitors (Fig. 3B, Table 1). After 48 h, cell yields (Fig. 3C) and ALDH1A1 transcription (Fig. 3D) was then measured. As expected, nordihydroguaiaretic acid (NDGA) and curcumin, both inhibitors of the AP-1 transcription complex which drives ALDH1A1 transcription[35], caused the greatest degree of ALDH1A1 inhibition accompanied by a moderate reduction in cell yield at some doses. Inhibition of JNK (SP600125) or p38 (SB203580) increased proliferation at low doses, with a modest reduction in ALDH1A1 transcription. RhoA inhibition (CT04) had no significant effect on proliferation and modestly reduced ALDH1A1 expression. Rac-1 has the capacity to inhibit RhoA[36], and its inhibition with NSC23766 had the expected effect of increasing proliferation accompanied by a modest reduction in ALDH1A1 transcription. Inhibition of β-catenin's capacity to activate TCF with inhibitor CCT036477 modestly increased proliferation, accompanied by a slight reduction of ALDH1A1 transcription. Inhibition of GSK3β with BIO is expected to accelerate cWnt signaling through

◄**Fig. 2**. Transcriptional blockade of Dkk-1 in MG63 OS cells attenuates proliferation, survival, osteoinhibition and ALDH1A1 expression. (**A**) ELISA measurement of Dkk-1 in media supernatants by MG63-kdDkk1 and MG63-scr cells. (**B**) Relative transcription of Dkk-1 by MG63-kdDkk1 and MG63-scr cells. (**C**) Cell density at the time of assay for panel A and B. (**D**) Proliferation under standard culture conditions. (**E**) Final cell density of MG63-kdDkk1 and MG63-scr cells after 10 days of nutrient (medium) deprivation under confluent conditions. (**F**) Final cell density of MG63-kdDkk1 and MG63-scr cells after 2 days of exposure to DRB. (**G**) Immunoblots of the phosphorylation status of RhoA, Mkk4, p30 and JNK in MG63-kdDkk1 and MG63-scr cells after 8 days of standard culture. (**H**) Immunoblot assays of ALDH1A1 from triplicate cultures of MG63-kdDkk1 and MG63-scr cells after 8 days of standard culture (above). Densitometric measurements of the triplicate bands normalized to GAPDH (below). (**I**) ELISA measurement of OPG in media supernatants by MG63-kdDkk1 and MG63-scr cells exposed to 5 days of osteogenic conditions. (**J**) Colorimetric assay of ALP activity in MG63-kdDkk1 and MG63-scr monolayers exposed to 8 days of osteogenic conditions. (**K**) ARS-stained monolayers of MG63-kdDkk1 and MG63-scr monolayers exposed to 5, 10 and 15 days of mineralizing osteogenic conditions. (**L**) Spectrophotometric measurement of ARS stain recovered from monolayers in Panel K. Statistics: Panel A-C, E, H-J: two-tailed student's *T*- test. **$p < 0.01$, ***$p < 0.005$, n = as indicated. Panel D, L: two-sided ANOVA. Panel F: one-sided ANOVA and Tukey's multiple comparison test. ***$p < 0.005$, n = 6.

stabilization of β-catenin. At the doses tested, BIO treatment increased the rate of cell proliferation. Although counter-intuitive, this observation suggests that the action of Dkk-1 and upregulated cWnt do not necessarily have opposing or exclusive roles in stimulation of OS growth. Overall, the implementation of small molecule inhibitors to modulate cell proliferation and ALDH1A1 expression yielded unpredictable outcomes in most cases (summarized in Table 2), highlighting the complexity of the mechanisms that contribute to cWnt/ncWnt homeostasis, especially at the level of intracellular signaling.

In confluent MOSJ-Dkk1 cultures, extracellular Dkk-1 levels peak at 20 ng.mL[−19], and the range in the blood of OS patients is 16.84–2210.14 ng.mL[−128]. The Dkk-1 targeting antibody BHQ880[37,38] was added to cultures at a stochiometric excess of approximately 6 and 60 fold (1 μg.mL^{−1} and 10 μg.mL^{−1}). After 2 days, BHQ880 cells failed to slow proliferation or deplete ALDH1A1 transcription even though this antibody is effective in reducing bone destruction animal models of MBD[38,39]. On the other hand, targeting the transcription of Dkk-1 using the cell-permeable antisense morpholino, DkkMo[27] dose-dependently reduced proliferation of MOSJ-Dkk1 cells and inhibited ALDH1A1 transcription (Fig. 3C,D and Table 2). From those agents tested, the results indicate that curcumin, NDGA or DkkMo provide the most reliable means to slow proliferation and ALDH1A1 transcription in MOSJ-Dkk1 cells.
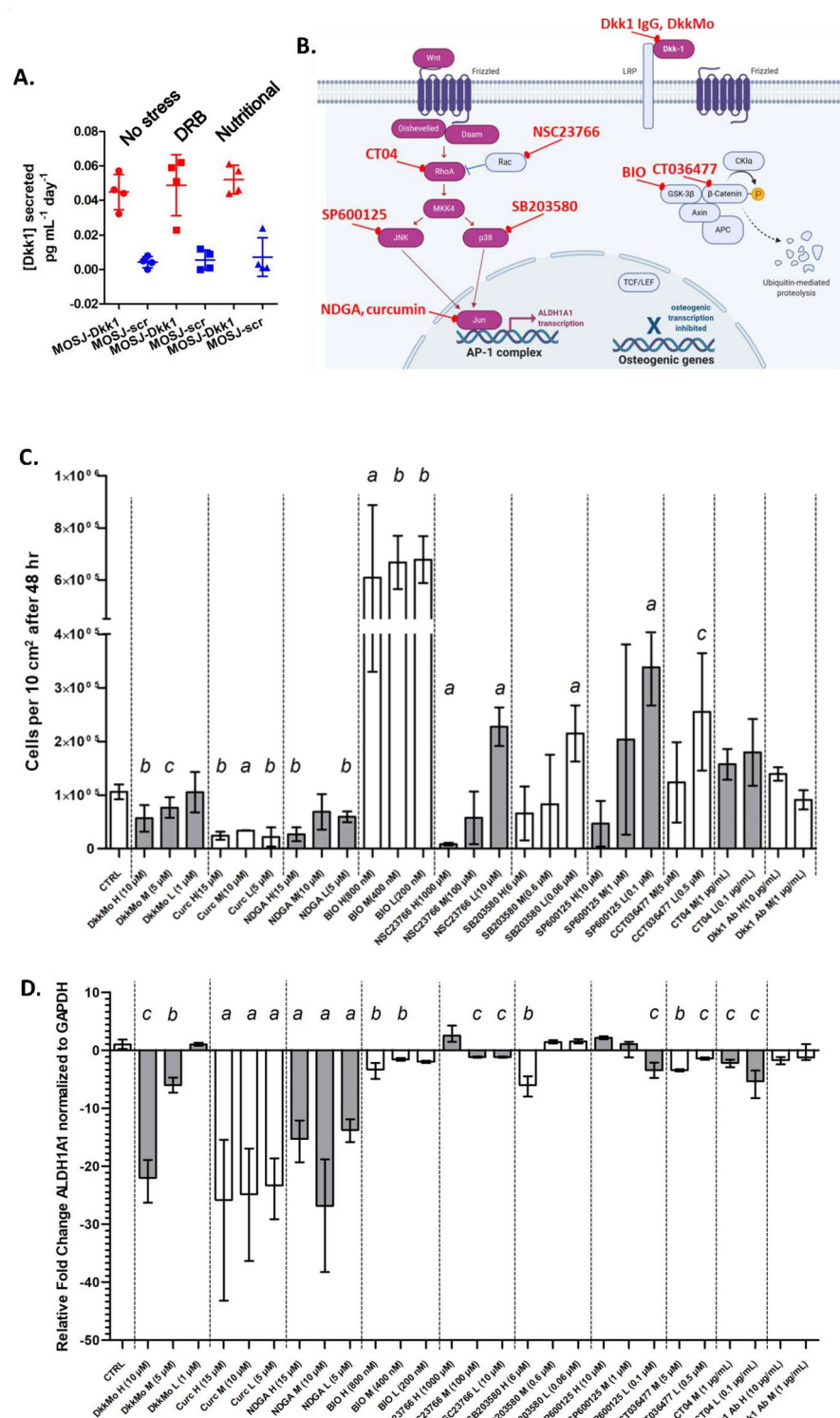
DkkMo slows proliferation of human cell lines and growth of patient derived xenografts in a 3D culture model of OS

We previously reported that 3D co-culture of OS cells with osteogenically enhanced human mesenchymal stem cells (OEhMSCs) in a rotating wall vessel (RWV) bioreactor provides an experimentally accessible means to study how OS cells interact with osteoprogenitors[40] (Fig. 4A). Green fluorescent protein-labeled OEhMSCs were loaded on collagen I-coated polystyrene microcarriers and subjected to 24 h of equilibration. Then dsRed labeled MG63 cells attached to identical microcarriers were added. DkkMo or scrambled control morpholino (scrMo) was added to cultures and incubated with replenishment of 50% medium and morpholino every 48 h. After 4 days, OEhMSCs and MG63 cells had undergone approximately 2.5 and 3.5 doublings respectively in the presence of scrMo (Fig. 4B). In the presence of DkkMo, the proliferation of MG63 cells was inhibited at the highest dose (10 μM) when compared with scrMo (Fig. 4B) but levels of OEhMSCs were unaffected. DkkMo significantly upregulated the ratio of secreted OPG:Dkk1 and the osteogenic biomarker ALP, when compared to the scrMo control (Fig. 4C, D) and ALDH1A1 expression was reduced (Fig. 4E). Collectively, these data indicate that DkkMo has the capacity to selectively inhibit the proliferation of human MG63 cells and upregulate molecular markers of osteogenesis.

Fragments (approximately 9 mm³) of the DAR human PDX-OS[41,42] were cultured for 8 days in the RWV with 10 μM scrMo or DkkMo. DkkMo began to blunt Dkk-1 output at day 2 (Fig. 4F), and this was associated with a reduction in mass (Fig. 4G, H) and glucose consumption (Fig. 4I). These data suggest that DkkMo has the capacity to significantly impact solid tumors in terms of Dkk-1 output, metabolism and growth.

DkkMo upregulates tumor necrosis while inhibiting bone destruction and pulmonary metastases

To examine the effect of DkkMo on OS disease parameters in vivo, an orthotopic OS model was established where the DAR PDX-OS was implanted adjacent to the femoral diaphysis of NSG mice. Some mice received intraperitoneal administration of 12.5 mg.kg^{−1} DkkMo[27], and untreated control mice received vehicle every 48 h. Tumor volume was measured by ultrasound over 12 days, indicating reduction in the kinetics of tumor growth (Fig. 5A), but tumor volume at endpoint, as measured by μCT, was not significantly reduced (Fig. 5B). DkkMo has been demonstrated to cause tumor necrosis in MOSJ-Dkk1 derived tumors that could be visualized by μCT[27], but these were not discernible for DAR tumors. To exclude the possibility that necrotic patches were invisible to μCT, closely aligned tumor biopsies were subjected in parallel to histology and genomic DNA quantification (Fig. 5C). Biopsies recovered from DkkMo treated tumors yielded significantly less DNA when compared to controls (Fig. 5D) and histological analysis of the adjacent biopsies indicated large patches devoid of cells in DkkMo-treated tumors that were sparsely represented in controls (Fig. 5E). The cells adjacent to the acellular patches exhibited pyknosis and nuclear fragmentation (karyorrhexis) characteristic of necrosis (Fig.

Fig. 3. DkkMo slows proliferation of MOSJ-Dkk1 cells and attenuates ALDH1A1 transcription. (**A**) Dkk-1 output by MOSJ-Dkk1 and MOSJ-scr cells after 2 days of exposure to doxorubicin (DRB) or nutritional deprivation. (**B**) Schematic of the putative PCP-like ncWnt pathway proposed to regulate Dkk-1-mediated ALDH1A1 expression[9,27] (*left*) and cWnt (*right*) pathway with inhibitor targets indicated. (**C**) MOSJ-Dkk1 yields after incubation with various concentrations of inhibitor as determined by qRT-PCR for GAPDH transcription. Annotations (*a-c*) refer to p-values (*a*: $p < 0.05$, *b*: $p < 0.01$, *c*: $p < 0.005$) compared to control standard culture conditions (CTRL) and H, M and L refer to high, medium and low dose respectively. (**D**) Fold-change ALDH1A1 transcription under conditions of panel B as determined by qRT-PCR using GAPDH as an internal control. Annotations (*a-c*) refer to p-values (a: $p < 0.05$, b: $p < 0.01$, c: $p < 0.005$) when compared to standard culture conditions. Statistics: Panel B-C: 1-sided ANOVA and Bonferroni multiple comparison test against control conditions only (n = 6).

Compound	Target	Mechanism	Ref
Bromoindirubin monoxime (BIO)	GSK3β	Prevents phosphorylation of GSK3β active site which in turn results in reduced phosphorylation of β-catenin resulting in its stabilization. Mimics cWnt activity	[44]
CCT03677	β-catenin and TCF	Blocks interaction between β-catenin and TCF	[45]
CT04	RhoA	Inhibits RhoA by ADP-ribosylation of effector binding domain of associated GTPase	[46]
Curcumin	AP-1 complex	Directly interacts with *fos* and *jun* dimers, preventing DNA binding	[47]
Anti Dkk-1 antibody	Dkk-1 ligand	Prevents binding of Dkk-1 to Frz or LRP5/6	[39]
DkkMo	Dkk-1 mRNA	Vivo morpholino blocks transcription of Dkk-1	[27]
NDGA	AP-1 complex	Directly interacts with *fos* and *jun* dimers, preventing DNA binding	[47]
NSC23766	Rac-1	Inhibits binding of Rac-1 to its guanine nucleotide exchange factor	[48]
SB203580	p38	Binds kinase and prevents downstream phosphorylation	[49]
SP600125	JNK 1 and 2	Competes with ATP binding to prevent activation of JNK	[50]

Table 1. List of agents used in MOSJ-Dkk1 assays.

Agent	Target	Proliferation	ALDH1A1
BIO	GSK3β	+++(ld, md, hd)	- (hd, md)
CCT036477	β-catenin and TCF	+(hd)	- (hd, md)
CT04	RhoA	nc	- (hd, md)
Curcumin	AP-1 complex	-- (ld, md, hd)	--- (ld, md, hd)
Anti Dkk-1 antibody	Dkk-1 ligand	nc	nc
DkkMo	Dkk-1 mRNA	-- (hd), - (md)	--- (hd), -- (md)
NDGA	AP-1 complex	- (hd)	--- (ld, md, hd)
NSC23766	Rac-1	-- (ld), +++(hd)	- (hd)
SB203580	p38	++(hd)	- (hd)
SP600125	JNK 1 and 2	++(ld)	- (ld)

Table 2. Summarized outcome of MOSJ-Dkk1 assays. +, ++, +++: upregulation, -, --, --- : downregulation. *nc* no change, *ld* at lowest dose, *md* at mid dose, *hd* at highest dose.

S1A, B) and were more significantly more numerous in DkkMo treated tumors (Fig. S1C). These data indicate that while tumor mass is modestly affected by DkkMo, tumor cells succumb to stressors that result in extensive necrosis and nuclear fragmentation.

The µCT scans indicated that the femurs of DkkMo treated mice exhibited less bone destruction that vehicle treated counterparts (Fig. 5F). To quantify this observation, 3D renderings of each diaphysis was subjected to calculations of the product of inertia (POI) to quantify the degree of asymmetry introduced by osteolysis. For a perfect cylinder, the POI for any plane is 0 and asymmetry causes deviation from 0. Contralateral diaphyses in either treatment group had a POI of 0.026 (SD 0.0042) in the plane (x, y) separating the lateral and medial sides (Fig. 5G, contralateral). Tumor-bearing femurs had a mean POI of 0.049 (SD 0.0115), but DkkMo treatment significantly reduced the mean and range (0.022, SD 0.0062) closer to contralateral values (Fig. 5G, ipsilateral). These data indicate that DkkMo administration reduced bone destruction caused by the PDX-OS.

It has been reported that immunological blockade of Dkk-1 can reduce pulmonary metastases in orthotopic human PDX-OS mouse models[41]. To examine whether DkkMo had the capacity to inhibit pulmonary metastases, mRNA from lungs excised from the PDX-OS recipient mice was subjected to qRT-PCR for human or murine GAPDH. Human GAPDH signal was normalized to murine pulmonary GAPDH and expressed as $2^{-\Delta CT}$. The $2^{-\Delta CT}$ signals were significantly elevated in vehicle-treated mouse lungs as compared to those treated with DkkMo (Fig. 5H). Furthermore seven of nine vehicle-treated mouse lungs bore detectable human GAPDH whereas two of ten DkkMo treated lungs bore detectable human GAPDH after treatment with DkkMo (Fig. 5I). Micro-metastases could be visualized on H&E-stained lung sections form vehicle treated tumors (Fig. 5J). Collectively, these data indicate that DkkMo has the potential to reduce probability and extent of pulmonary metastases by PDX-OS tumors.

DkkMo inhibits OS progression in part by stimulation of tissue regeneration, inhibition of the cell-cycle and reduced infiltration of inflammatory cells

The tumors and tissue margins of three specimens from each treatment group were subjected to single-cell RNA sequencing. Tumor and host stromal sequences were mapped against a human or murine reference genome respectively (Fig. 6A). Principal component analysis (PCA) and clustering was performed on the pooled datasets based on differential gene expression analysis (DGEA) (Fig. S2, S3). In the case of tumor reads, seven clearly defined clusters were identified that separated DkkMo treated cells from vehicle-treated cells (Fig. 6B, Fig. S2). Clusters that harbored predominantly vehicle treated cells (1, 3, 4, 6) were also enriched for cells in the G2M and S-phase of the cell cycle with fewer cells harboring a G1 signature (Fig. 6C). The converse was true for clusters
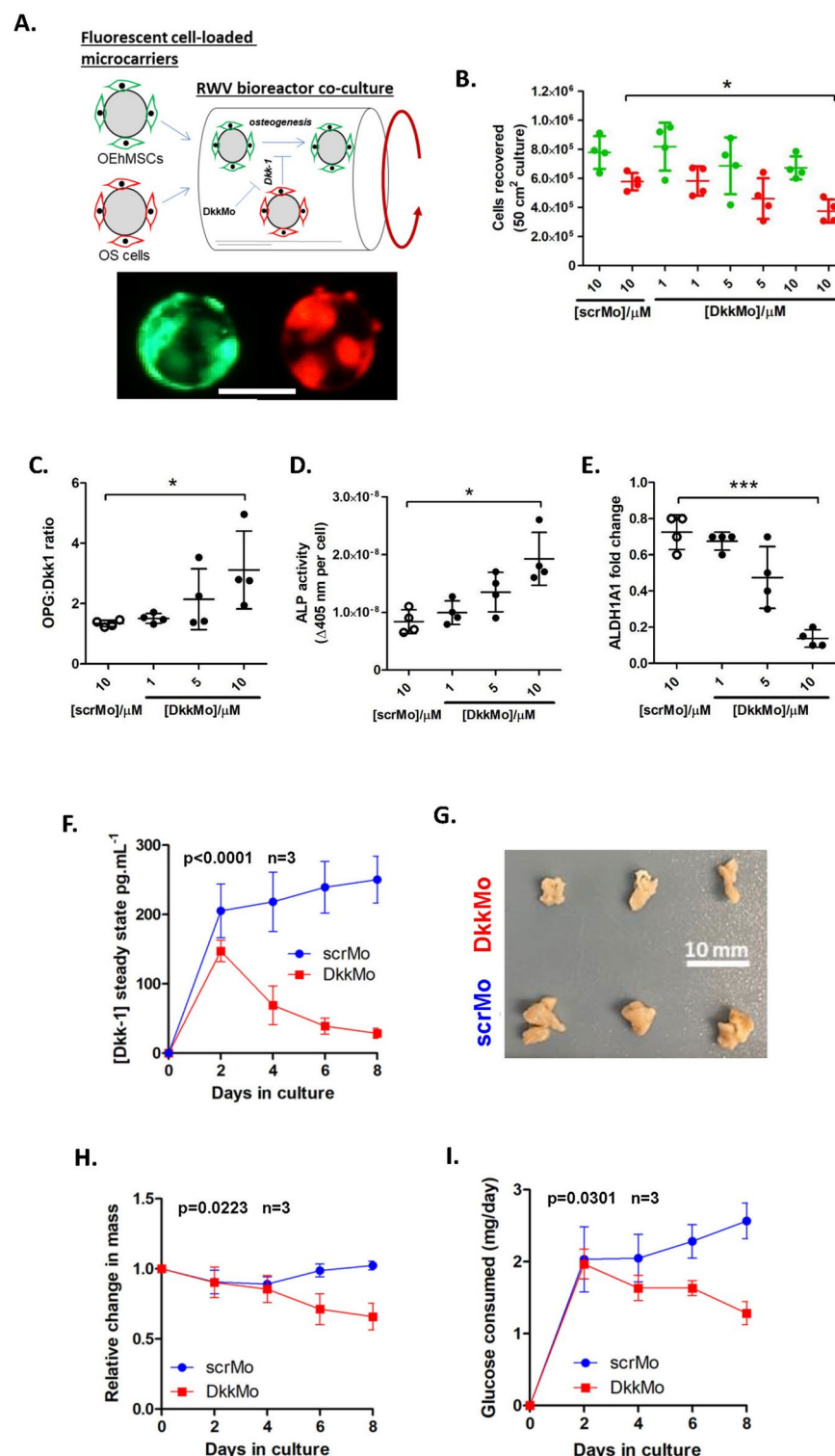
containing predominantly DkkMo treated cells (cluster 0, 2 and 5), with most cells in these clusters expressing a G1 cell cycle signature (Fig. 6C). When clusters were plotted based on the proportion of cells expressing a G1 signature versus the proportion of DkkMo treated cells, the proportion of DkkMo treated cells correlated with G1 status, demonstrating that DkkMo treatment is a negative determinant of cell-cycle entry (Fig. 6D). Each cluster was also analyzed for tissue expression and gene ontology (GO) enrichment signatures. The clusters enriched for vehicle treated cells upregulated endothelial, fibroblastoid, dendritic, and keratinocyte tissue signatures (Fig. 6E). GO enrichment analyses (Table 3) indicated vehicle-treated cells exhibited upregulated hormone responses (cluster 1, Fig. S3), gene transcription (cluster 3), proliferation (cluster 4, Fig. S3), and MAPK kinase activity (cluster 6). In contrast, clusters enriched for DkkMo-treated tumor cells (clusters 0, 2, 5) were enriched for tissue signatures related to tissue regeneration including those related to osteogenic, endothelial, dermal, smooth muscle and fibroblastoid cell types (Fig. 6E). GO enrichment (Table 3) was primarily related

◀**Fig. 4**. DkkMo attenuates OS cell proliferation, reduces ALDH1A1 expression and osteoinhibition in 3D in vitro models of human malignant bone disease. (**A**) Schematic of the RWV-microcarrier-based co-culture OS model based on McNeill et al.[82]. Fluorescent micrographs of GFP-labeled OEhMSCs and RFP labeled MG63 laden microcarriers used in all experiments are presented below (bar = 100 μm). (**B**) OEhMSC (green) and MG63 (red) cell yields after 8 days of coculture in the RWV with DkkMo or scrMo. (**C**) OPG:Dkk-1 ratios measured on media supernatants from cultures in panel A. (**D**) ALP activity of cell-laden microcarriers from cultures in panel A. (**E**) ALDH1A1 transcription by cells attached to microcarriers from cultures in panel A, compared to control cultures that received no morpholino. (**F**) Dkk-1 output by PDX specimens cultured as whole morsels in the RWV with 10 μM DkkMo or scrMo. (**G**) Appearance of PDX tumors after 8 days of culture. (**H**) Relative change in mass (compared to initial mass at day 0) over 8 days of culture. (**I**) Glucose consumption over 8 days of culture. Statistics: Panel B: 1-sided ANOVA and Tukey's multiple comparison test. * $p < 0.05$, n = 4. (**C–E**) One-sided ANOVA and Bonferroni multiple comparison test (vs. scr). *$p < 0.05$, ***$p < 0.005$, = 4. (**F,H,I**) two-sided ANOVA, p and n indicated.

to tissue regeneration, ECM synthesis and osteogenesis for all DkkMo treated groups (Fig. S3). The largest proportion of DkkMo-treated cells were classified in cluster 0, highly enriched for genes related to connective tissue regeneration (Fig. 6F).

In the case of the murine tumor stroma reads, DkkMo and vehicle treated cells partitioned into some clusters that could also be distinguishable by treatment group (Fig. 6G). As with the tumor cells, the three clusters that were enriched for vehicle-treatment (clusters 1, 3, 5) bore the majority of the cells in G2M and S-phase whereas clusters enriched for DkkMo-treated cells (0, 4, 6) were enriched for G1 cells (Fig. 6H, I). Clusters that enriched for vehicle treatment contained immune cells such as T-cells (cluster 1), macrophages, dendritic cells and neutrophils (clusters 3 and 5) (Fig. 6J) whereas clusters with the majority of DkkMo-treated cells exhibited tissue regenerative signatures such as fibroblasts, endothelial cells, pericytes and smooth muscle cells (Fig. 6J, K). GO enrichment analysis (Table 4) indicated involvement of vehicle-treated cells (clusters 1, 3 and 5) with immune responses, with upregulation of genes related to immune cell chemotaxis, antigen processing and inflammation respectively. Clusters enriched for DkkMo treatment were associated with regenerative processes (Table 4) such as osteogenesis and ECM synthesis (cluster 0, Fig. 6K), angiogenesis (cluster 0, 6), and interestingly accelerated aerobic respiration and respiratory chain assembly (cluster 4) (Fig. S5).

Collectively, these data indicate that vehicle-treated tumor cells are enriched for signatures related to cell cycle progression and in some cases tumor survival, whereas DkkMo treatment caused tumor cells to remain in the G1 phase of the cell cycle while upregulating genes related to tissue generation. The tumor stroma of vehicle-treated samples also harbors a greater number of cycling and immunologically active cells, and like tumor cells, the introduction of DkkMo is associated with G1 cell-cycle arrest and the upregulation of regenerative processes. Collectively speaking, DkkMo appears to shift tumor and stroma from a cycling inflammatory state to a proliferatively more quiescent and regenerative mode.

Spatial transcriptomic analyses of human (tumor) transcripts were performed on representative specimens for the vehicle treated and DkkMo-treated groups. In the case of DkkMo treatment (Fig. 7, left), transcripts related to collagen and heterotypic fibril formation was heavily represented (zone D1), corresponding closely to cluster 0 of the single-cell sequencing data set. Interestingly, genes related to muscle differentiation was heavily represented in the periphery of the tumor where the masses are most likely to contact host muscle tissue. Vehicle treated tumors (Fig. 7, right) possessed zones enriched for expression of survival factors (zone V1) similar to cluster 4 identified by single-cell sequencing. There was also a large zone with enriched markers of cell migration and TGFβ signaling (zone V3) which may represent those cells with increased metastatic potential and an isolated patch on the periphery of the tumor with elevated expression of muscle markers and oxidative phosphorylation.

Discussion

Dkk-1 serves contradictory roles in the etiology of malignancy[43,44–50]. The secreted ligand was originally discovered as an inhibitor of the cWnt signaling pathway[51], which is known to drive survival and proliferation in diverse tissue systems[52,53]. Not surprisingly, the cWnt pathway harbors proto-oncogenes[54] and as such, Dkk-1 is often regarded as a tumor suppressor[55]. In OS, this interpretation has been supported by reports of nuclear β-catenin accumulation histological sections[56,57] and antagonism or silencing of Wnt inhibitor expression in tumors[58–60]. In spite of these observations, the role of cWnt in driving OS progression is less definitive than in other malignancies[61], and mutations known to cause oncogenic activity of β-catenin in soft tissue tumors have not been identified in OS[56,57]. To further challenge a tumor-suppressing role for Dkk-1 in OS, inhibition of β-catenin activity can enhance motility and metastases[62], activation of cWnt suppresses OS metastases[63], and activation cWnt can blunt OS proliferation[64]. Dkk-1 is known to disrupt the balance between cWnt and ncWnt signaling in favor of the latter[9,17,18,27,65], resulting in transformation of mesenchymal stem cells to pleiomorphic sarcomas[66], exacerbating the malignancy of murine OS[27,67], and driving malignancy of canine prostate cancer[17,18] through JNK dependent mechanisms. Expression of Dkk-1 is also high in the blood of OS patients and its expression is highest in the mitotic periphery of human OS tumors[28]. Dkk-1 also activates AKT and NF-κB signaling via direct engagement of the cytoskeleton-associated protein 4 (CKAP4)/p63 receptor[68–70] and OS progression has been linked to dysregulated CKAP4 activity[71]. Overall, predicting the roles of cWnt and Dkk-1 in malignancies without empirical evidence is challenging, but Dkk-1 while correlates with a tumor-suppressor role in endodermal and ectodermal tissues the converse appears to be true for tumors of mesodermal origin such as bone[43].
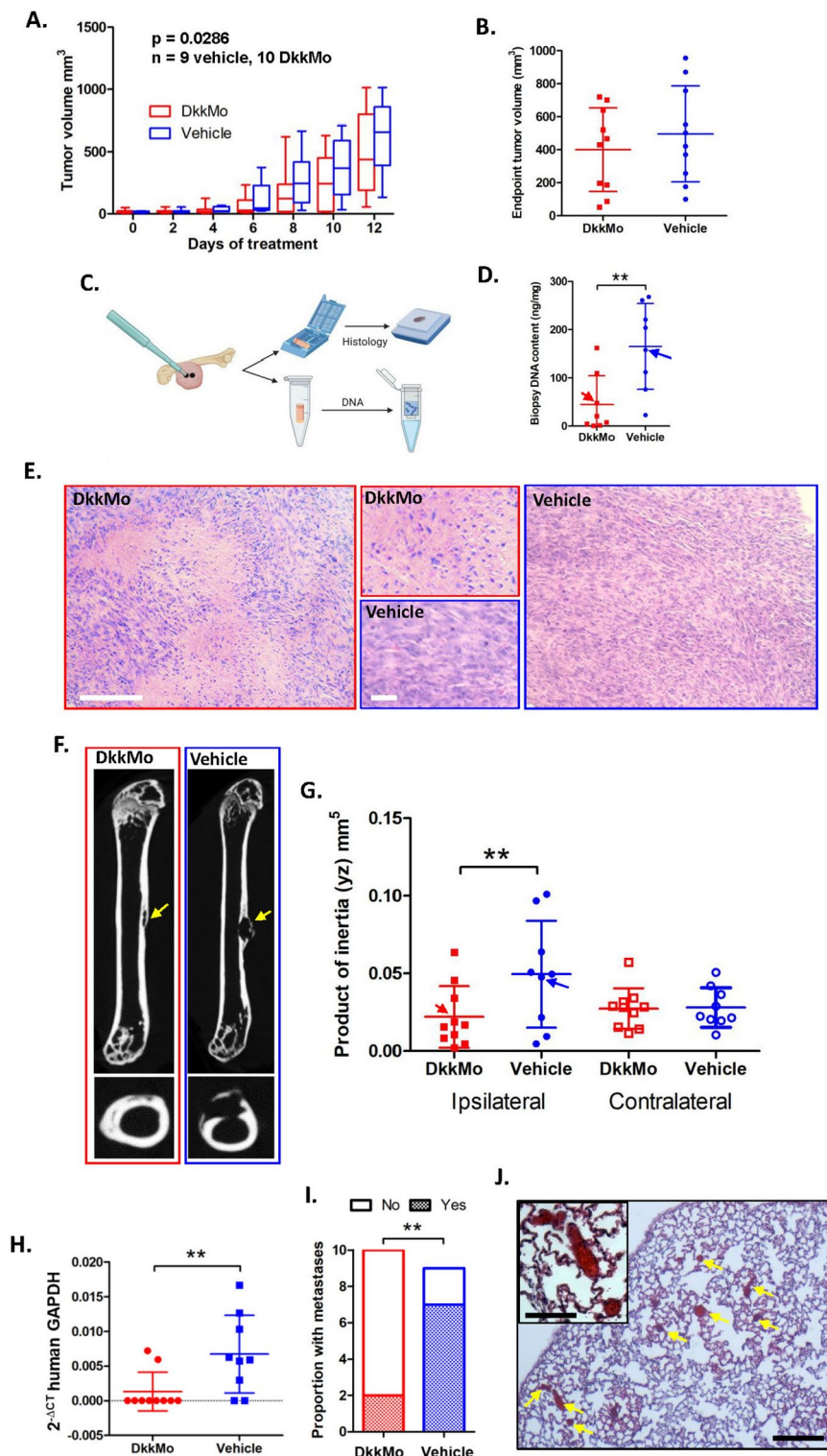
Previously, we demonstrated that constitutive expression of human Dkk-1 in the osteogenic OS cell line MOS-J reduced osteogenic differentiation and drastically accelerated bone destruction in grafts[9]. The Dkk-1 expressing MOSJ-cells (MOSJ-Dkk1) also produced larger, more aggressive tumors[9]. We found this effect was caused in part by upregulation of ALDH1A1, a stress response protein and driver of tumor survival[19,20], and that the upregulation was caused by a Dkk-1 mediated shift in the balance between cWnt and ncWnt signaling resulting in upregulation of JNK mediated pathways[9]. When Dkk-1 expression was ablated by DkkMo, MOSJ-DkkMo tumors grew slower and were more necrotic than controls[27]. Dkk-1 mediated survival signals have been predicted to exist in MSCs[29], prostate cancer cells[17,18], OS cells[29], and patient derived xenografts[41]. Proliferation induces replication stress, especially after transformation[72,73], and it has been proposed that Dkk-1 expression is a prerequisite to entry into the cell cycle to activate stress mitigation pathways[29,74]. Resultant upregulation of ALDH1A1 in this instance would be predicted to counter the effects of oxidative stress[19,75] and DNA damage[76].

◀**Fig. 5**. DkkMo inhibits tumor growth and survival, rate of metastasis, and bone destruction in a murine orthotopic model of human OS. (**A**) Tumor volume measured by ultrasound imaging. Columns represent upper to lower quartile measurements, the central line represents median, and error bars represent full range of data. (**B**) Tumor volume at endpoint measured by μCT imaging. (**C**) Schematic of sampling protocol for analysis of tumor necrosis. (**D**) Measurement of DNA content in tumor biopsies. Arrows indicate samples presented in panel E. (**E**) H&E-stained histology of adjacent biopsy. Large outer images are low power (*bar* = 500 μm) and smaller central images are high power (*bar* = 100 μm). (**F**) Representative μCT reconstructions of femurs with the yellow arrow indicating site of tumor interaction with the bone. The axial orientation at the point of the arrow is presented below in each case. (**G**) Product of inertia measurements for ROI corresponding to the diaphysis in contact with the tumor. Arrows indicate samples presented in panel F. (**H**) Pulmonary metastases detected by qRT-PCR for human GAPDH. Values are normalized to murine GAPDH and presented as 2^{-dCT}. (**I**) Frequency of metastases. (**J**) Vehicle-treated lung section stained with H&E, displaying micro-metastases. *Bar* = 100 μm main image, 20 μm inset. Statistics: Panel A: two-sided ANOVA, p and n indicated. Panel B, D, G: two-tailed student's *T*- test. **p < 0.01, n = as indicated. (**H**) Two-tailed student's *T* test on arcsine transformed data **p < 0.01, n = as indicated. (**I**) Fisher exact test **p < 0.01, n = 9.

In this study, Dkk-1 secretion was found to be maximal in proliferative OS cells but reduced at high density when contact inhibition had slowed proliferation. Dkk-1 secretion was concomitant with JNK and ALDH1A1 upregulation suggesting that like MOSJ-Dkk1 cells, Dkk-1 activates ALDH1A1 via a JNK-mediated ncWnt pathway. To examine whether Dkk-1 expression could be triggered by other stressors, confluent OS cells with minimized Dkk-1 output were exposed to ROS induced by addition of H_2O_2. While H_2O_2 caused cell death, Dkk-1 levels were not substantially upregulated suggesting that the presence of ROS alone is not sufficient to trigger Dkk-1 expression in OS cells. DRB is used frequently as one of the adjuvant agents in the treatment of OS[77] and while its mechanism of action is complex, DNA damage and ROS generation are regarded as the major cytotoxic drivers[30]. With DRB exposure, Dkk-1 output was rapidly upregulated, suggesting that the triggers of Dkk-1 expression include the DNA damage response[78,79] as well as cell-cycle activity.

The shRNA-mediated knockdown of Dkk-1 caused a reduction in phosphorylated MKK4, p38 and levels of RhoA and ALDH1A1 indicating that Dkk-1 drove ALDH1A1 expression via a similar PCP-like ncWnt pathway to that observed in MOSJ cells[9,27]. Targeting of RhoA, JNK and p38 with specific inhibitors resulted in complex and unpredictable effects on cell growth and ALDH1A1 expression suggesting complex crosstalk in the cytosol. In contrast, direct inhibition of the AP-1 Jun-responsive element with curcumin or NDGA or direct blockade of Dkk-1 transcription with DkkMo all had the expected effect of reducing ALDH1A1 transcription and cell growth.

In human clinical trials, DKN-01, a Dkk-1 targeting IgG4 demonstrated efficacy in metastatic prostate[80] and endometrial carcinoma[81] and the anti-Dkk-1 monoclonal antibody BHQ880 has the potential to target Dkk-1 in MM[37]. Infusions of the BHQ880 monoclonal antibody had a positive effect on vertebral bone density in patients suggesting that an antibody-mediated approach could enhance bone anabolism but repair of bone lesions was modest, suggesting that BHQ880 failed to deplete Dkk-1 in osteolytic lesions where concentrations are expected to be much higher[28]. The bioavailability of BHQ880 is also likely to be diminished by high levels of Dkk-1 in the blood where levels can reach hundreds of μg.mL$^{-18,28}$. DkkMo, on the other hand, which targets the Dkk-1 transcript, is not likely to be affected by circulating Dkk-1 and it is well tolerated in a preclinical murine model[27].

Initial experiments were performed in a 3D microcarrier system designed to mimic OS MBD where MG63 OS cells were co-cultured with OEhMSCs. The OEhMSCs were employed to serve as osteoprogenitors in the system[82]. In the presence of inactive morpholino, the ratio of the osteogenic ligand OPG compared to Dkk-1 was low resulting in reduced osteogenesis in the system. However, when DkkMo was added, Dkk-1 levels dropped, raising the OPG:Dkk-1 ratio and increasing osteogenic activity. With increased DkkMo dosage, ALDH1A1 levels and MG63 cell numbers were both reduced, but OEhMSCs were not substantially diminished, suggesting that OS cells are more susceptible to adverse growth conditions that arise from the reduction in ALDH1A1. When specimens of human PDX-OS were incubated with DkkMo, Dkk-1 levels in the medium dropped sharply to near-undetectable levels. This is not unexpected given that while the PDX-OS specimens were irregular in shape, the tissue thickness was on average 2–5 mm, similar to the spacing of the microvasculature[83] and within the limits of diffusion in solid tissues[84]. Vivo morpholino tissue penetration is also efficient[85] and the majority of Dkk-1 expression confined to outer periphery of OS tumors[28]. Tumor growth and glucose utilization was also inhibited by DkkMo indicating diminished tumor viability[86].

In the orthotopic PDX-OS model conducted in mice, *prima facie* measurements indicated that DkkMo only modestly affected tumor size, but histological and molecular analysis indicated hallmark signs of necrosis including profound pyknosis, karyorrhexis and chromatin degradation. DNA levels were reduced threefold in DkkMo-treated tumors, indicating that necrosis was widespread. Necrosis is a key indicator of neoadjuvant therapy success and a predictor of favorable prognosis in OS[4]. Bone destruction is virtually universal in OS and severity is correlated with metastases and poor prognosis[2]. DkkMo significantly reduced both bone destruction and the probability of pulmonary metastases. In the case of mitigating bone destruction, this is not unexpected given the pivotal role of cWnt signaling in the differentiation of MSCs to osteoblasts[7] and the potency of Dkk-1 in disrupting this process[8,9]. The mechanism by which Dkk-1 stimulates metastases is based to some extent on the destruction of peritumoral extracellular matrix that is driven by hyperactivity of local osteoclasts resulting in release of OS cells and pro-tumor factors into the circulation[2], but studies also indicate that perturbed cWnt activity can enhance migratory and metastatic tendencies in OS cells[62,63] and ALDH1 activity is correlated with
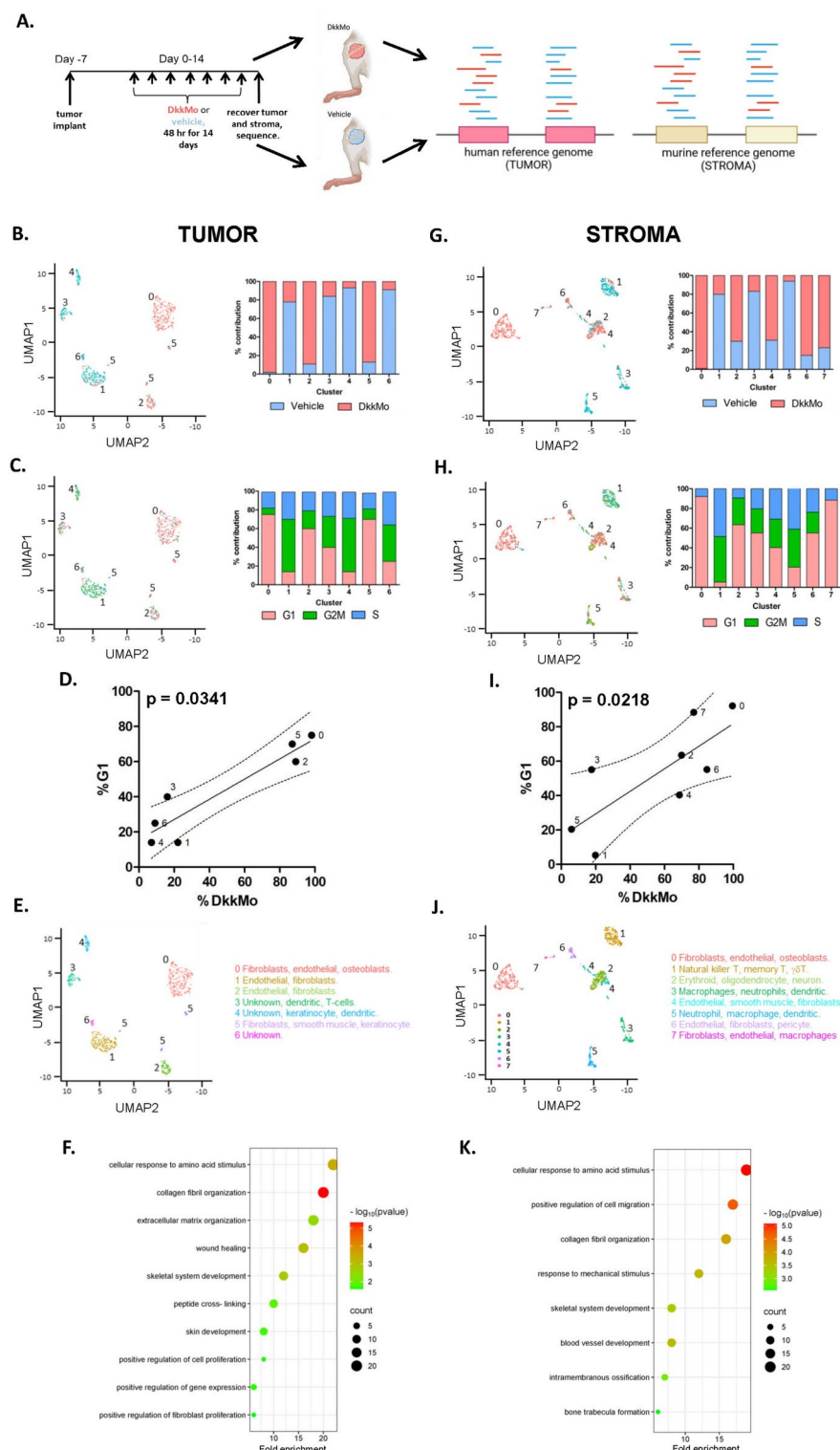
metastases in OS[87]. It noteworthy that migratory and metastatic markers related to TGF signaling[88,89] detected by single-cell and spatial expression analyses were upregulated in control but not DkkMo treated tumors. Collectively, these data suggest that DkkMo may have utility as an adjuvant agent for the inhibition of bone destruction and metastases, targeting two key mortality drivers in OS.

Single-cell transcriptomic analysis of the tumors and stroma was challenging due to the dense extracellular matrix and high levels of necrosis present in the DkkMo treated specimens but it was achievable. In the case of tumor tissue, DkkMo caused upregulation of osteogenic and tissue regenerative genes, suggestive of reinitiated osteoblast characteristics which is favorable given that poor prognosis correlates with a dedifferentiated phenotype[3]. On the other hand, untreated tumors were enriched for expression of growth factor pathway components and cell replication. Analysis of the tumor stroma indicated that DkkMo treatment caused the upregulation of osteogenic and tissue regenerative processes suggesting that DkkMo has a regenerative effect

◀**Fig. 6.** DkkMo promotes osteogenesis and tissue repair and reduces cell cycle activation in a murine orthotopic model of human OS. (**A**) Schematic of experimental strategy. (**B**–**F**) Analysis of human tumor transcripts mapped to human reference genome. (**G**–**J**) Analysis of murine stromal transcripts mapped to murine reference genome. (**B**) UMAP clustering (left) of single-cell sequences of human origin derived from OS tumors with treatment status (DkkMo or vehicle) indicated. Each cluster plotted (right) with the relative proportion of vehicle or DkkMo-treated cells. Panel C: UMAP plot reproduced from Panel A with annotation for cell-cycle status (left). Each cluster plotted (right) with the relative proportion of G1, G2M or S phase cells. (**D**) For each cluster, the proportion of DkkMo treated cells plotted against proportion in G1 is plotted. Trend line refers to least-squares fit with 95% confidence intervals indicated by curved lines. P-values refer to Spearman correlation analysis. (**E**) UMAP plot reproduced from Panel A with color coded clusters (left) with top three tissue signatures (by p-value) for each cluster. (**F**) Bubble plot of gene ontologies associated with cluster 0 demonstrating enrichment for connective-tissue regenerative signatures. (**G**–**K**) As Panel B-F, but analysis of murine stroma transcripts mapped to murine reference genome.

on bone tissue and angiogenic endothelia. On the other hand, vehicle-treated stroma was enriched for cells that expressed transcriptomic signatures related to innate immunity and inflammation with representation by natural killer T-cells, neutrophils and macrophages. While this observation was initially surprising given that the NSG mouse hosts are highly immune compromised, the strain used in this study has been reported to possess low levels of cytotoxic T cell activity[90] and appreciable levels of macrophages, dendritic cells and neutrophils[90–92]. It is therefore possible that DkkMo exhibits anti-inflammatory effects that could be beneficial in OS. Indeed, Dkk-1 has been reported to drive inflammatory cytokine responses[93], stimulate neutrophilic inflammation[94] and is correlated with chronic inflammation in sickle cell and Crohn's disease[95,96]. This observation is clinically significant because systemic markers of inflammation[97,98] and neutrophil infiltration[99,100] correlate with poor prognosis in OS. This preliminary observation should be regarded with some caution however, given the documented pleiotropic role of Dkk-1 with respect to immune regulation in malignancy[101].

Spatial transcriptomic analyses further demonstrated the effect of DkkMo in upregulation of osteoblast and tissue healing transcripts and in controls, indicated the increased presence of tumor expansion, migration and survival markers. An unexpected finding was the expression of human muscle differentiation and functional markers in tumor cells at locations adjacent to host muscle tissue. Given that these transcripts were of human origin, the signal could not have arisen from migratory myocytes or muscle tissue. The mechanism behind this interesting observation is uncertain but OS cells have been documented to exhibit pluripotency[102] and fusion with myofibroblasts[103].

This work provides significant insight into the potential effects of Dkk-1 antisense therapy in reducing the progression of osteosarcoma but there are limitations to the study. The DAR PDX-OS was specifically selected because the results from DkkMo could be compared to previously published studies with the monoclonal antibody BHQ880[41]. However, additional studies should be performed using different PDX samples with various degrees of Dkk-1 expression and histological characteristics. The study does not recapitulate a fully functional immune system and with it becoming increasingly apparent that Dkk-1 has the capacity to profoundly affect immune responses, future work with spontaneous genetic OS models in immune competent hosts is warranted.

Herein we demonstrate that blockade of Dkk-1 expression with a cell permeable vivo morpholino (DkkMo) inhibits key determinants of OS morbidity including tumor survival, bone destruction, metastases and immune cell infiltration. While the role of Dkk-1 in malignancy is complex and multi-faceted[43], these findings support the increasingly credible notion that the classical cWnt inhibitor has the potential to drive malignancy in interconnected ways. Vivo morpholinos have a favorable safety profile and can be manufactured at scale. Targeting of the Dkk-1 transcript rather than the ligand has the potential to overcome challenges associated with functional depletion due to high circulating levels of target. Collectively, these preclinical studies indicate that DkkMo demonstrates potential to serve as an effective adjuvant therapy for the treatment of highly malignant OS in humans and animals.

Methods
Reagents and biological materials
DkkMo and scrMo were custom synthesized by Gene Tools LLC (Philomath, OR). MG63 and SAOS-2 OS cells were acquired from the American Type Culture Collection (Manassas, VA). INA6 MM cells were a gift from John Shaughnessy, University of Arkansas Medical School. The DAR PDX-OS specimen (Chand Khanna, National Cancer Institute, Bethesda, MD) was a gift from David Loeb, Albert Einstein College of Medicine, New York. Bone marrow derived MSCs were acquired from the Texas A&M Stem Cell distribution core and utilized under an institutionally approved protocol. Dkk-1 targeting and scrambled shRNA lentiviral particles, polybrene and puromycin were acquired from Santa Cruz Biotechnology (Dallas, TX). H_2O_2 was purchased from Millipore-Sigma (Burlington, MA). DRB was purchased from Teva USA (Parsippany, NJ). Fluorescent labeling lentiviral particles (GFP and dsRed-tomato) were acquired from Takara Bio (San Jose, CA). BIO, CCT03677, curcumin, NDGA, NSC23766, SB203580, SP600125 were acquired form Calbiochem. CT04 cell permeable RhoA inhibitor was acquired from Cytoskeleton Inc. (Denver, CO). BHQ880 recombinant human Dkk-1 blocking antibody was acquired from Creative Biolabs (Shirley, NY). Doxorubicin was used at 10^{-8} mM as previously described[27].

Culture of OS and MM cells
OS cells were cultured in alpha-minimal-essential-medium (αMEM, Life Technologies, Carlsbad, CA) supplemented with 10% (v/v) fetal bovine serum (FBS, Premium Select, R&D Systems, Minneapolis, MN), 100

Group 0 (DkkMo)	p-value
Collagen fibril organization	4.70E-06
Cellular response to amino acid stimulus	3.80E-04
Wound healing	8.80E-04
Skeletal system development	1.60E-03
Extracellular matrix organization	3.30E-03
Peptide cross-linking	1.30E-02
Skin development	1.90E-02
Positive regulation of gene expression	2.30E-02
Positive regulation of cell proliferation	2.50E-02
Positive regulation of fibroblast proliferation	2.60E-02
Group 1 (vehicle)	
Cellular response to corticotropin-releasing hormone stimulus	2.30E-03
Cellular response to extracellular stimulus	8.80E-03
Intracellular receptor signaling pathway	1.60E-02
Negative regulation of protein ubiquitination	2.70E-02
Negative regulation of ERK1 and ERK2 cascade	3.80E-02
Fat cell differentiation	3.80E-02
Negative regulation of transcription from RNA polymerase II promoter	7.70E-02
Group 2 (DkkMo)	
Angiogenesis	4.50E-03
Negative regulation of endothelial cell proliferation	1.60E-02
Cellular response to hormone stimulus	1.80E-02
Receptor internalization	2.10E-02
Skeletal muscle tissue development	2.20E-02
Vasculogenesis	2.60E-02
Negative regulation of BMP signaling pathway	2.90E-02
Regulation of cell growth	3.30E-02
Cell differentiation	3.30E-02
Calcium ion transport	3.60E-02
Group 3 (vehicle)	
Negative regulation of transcription from RNA polymerase II promoter	3.60E-02
Regulation of gene expression	8.00E-02
Group 4 (vehicle)	
Positive regulation of cell proliferation	2.00E-02
Cellular response to tumor necrosis factor	5.60E-02
Regulation of cell proliferation	7.00E-02
Cell proliferation	7.10E-02
Group 5 (DkkMo)	
Positive regulation of cell migration	5.00E-03
Smooth muscle contraction	9.00E-03
Cell adhesion	2.10E-02
Positive regulation of cell adhesion	2.50E-02
Muscle contraction	3.60E-02
Response to virus	4.40E-02
Actin filament organization	6.20E-02
Response to hypoxia	7.00E-02
Endoderm formation	2.00E-03
Group 6 (vehicle)	
Endoderm formation	2.00E-03
Negative regulation of MAPK cascade	6.90E-03
Protein dephosphorylation	1.90E-02

Table 3. Gene ontology enrichment analysis of human OS cell clusters.

Group 0 (DkkMo)	p-value
Wound healing	4.60E-07
Cellular response to amino acid stimulus	8.40E-06
Positive regulation of cell migration	2.00E-05
Collagen fibril organization	1.20E-04
Response to mechanical stimulus	2.20E-04
Blood vessel development	2.50E-04
Skeletal system development	4.50E-04
Intramembranous ossification	1.20E-03
Bone trabecula formation	2.70E-03
Group 1 (vehicle)	
Positive regulation of natural killer cell chemotaxis	1.70E-03
Positive regulation of cell–cell adhesion mediated by integrin	2.40E-03
Positive regulation of T cell chemotaxis	5.10E-03
Eosinophil chemotaxis	8.90E-03
Lymphocyte chemotaxis	1.10E-02
Monocyte chemotaxis	1.30E-02
Chemokine-mediated signaling pathway	1.80E-02
Positive regulation of cell adhesion	2.50E-02
Neutrophil chemotaxis	2.80E-02
Cellular response to interleukin-1	2.80E-02
Group 2 (mixed)	
Erythrocyte development	3.20E-07
Oxygen transport	1.10E-05
Cellular oxidant detoxification	4.80E-05
Hydrogen peroxide catabolic process	7.00E-05
In utero embryonic development	9.90E-03
Glutathione metabolic process	3.30E-02
Group 3 (vehicle)	
Antigen processing and presentation of exogenous peptide antigen via MHC class II	8.50E-03
Killing of cells of other organism	3.40E-02
Defense response	4.60E-02
Group 4 (DkkMo)	
Mitochondrial ATP synthesis coupled proton transport	2.00E-04
Mitochondrial respiratory chain complex I assembly	2.10E-04
Aerobic respiration	2.60E-04
Group 5 (vehicle)	
Neutrophil chemotaxis	1.70E-08
Inflammatory response	4.30E-04
Positive regulation of inflammatory response	6.70E-04
Immune system process	1.10E-03
Chemotaxis	1.20E-03
Peptide secretion	1.60E-03
Neutrophil aggregation	1.60E-03
Positive regulation of peptide secretion	2.00E-03
Response to lipopolysaccharide	2.30E-03
Peptidyl-cysteine S-nitrosylation	2.40E-03
Group 6 (DkkMo)	
Positive regulation of angiogenesis	4.00E-02
Positive regulation of cell migration	6.40E-02
Angiogenesis	7.00E-02
Group 7 (mixed)	
Chemotaxis	9.30E-04
Apoptotic process involved in luteolysis	1.00E-03
Axon guidance	1.80E-03
Telencephalon cell migration	2.40E-03
Very-low-density lipoprotein particle remodeling	2.40E-03
Continued	

Roundabout signaling pathway	2.70E-03
Positive regulation of ERK1 and ERK2 cascade	2.90E-03
Negative regulation of dendritic cell apoptotic process	5.50E-03
Pulmonary valve morphogenesis	6.20E-03
Cell adhesion	1.60E-02

Table 4. Gene ontology enrichment analysis of murine stroma cell clusters.

U.mL^{-1} penicillin & 100 μg.mL^{-1} streptomycin (Life Technologies) and 2 mM L-glutamine (Life Technologies). For expansion, cells were seeded at 500 cells per cm^2 with media changes every two days. Adherent cells were recovered using 0.25% (w/v) trypsin/ethylene diamine tetra-acetic acid (EDTA) (Life Technologies) when a density of approximately 80–90% confluency was reached. For growth curves, cells were plated at an initial density of 500 cells per cm^2 and allowed to proliferate for 15 days with changes of media every 2 days. At day 5, 10 and 15, medium was recovered for Dkk-1 ELISA and cells were recovered for enumeration by hemocytometer or by Cyquant fluorescent DNA quantification dye as previously described[104]. INA6 cells were grown in suspension culture as previously described[105]. For experiments, INA6 cells were seeded at a density of 5000 cells per mL and cultured for 15 days. Cultures were visualized by phase contrast microscopy was using a Nikon Eclipse TS100 and NIS Elements software (Melville, NY). In all cases, DRB was added to cultures at day 13 at a concentration of 0.25 μM[106], and H$_2$O$_2$ was added to cultures at day 13 at a concentration of 100 μM[107]. For shRNA-mediated Dkk-1 knock-down experiments, MG63 cells were cultured to the logarithmic phase of growth (approximately 5,000 cells per cm^2) and lentivirus was added at a multiplicity of infection (MOI) of 30 with 9 μg.mL^{-1} polybrene. After 2 days of virus exposure, cultures were washed twice in PBS and selected by addition of 8 μg.mL^{-1} puromycin for 5 days and 5 μg.mL^{-1} for a further 5 days.

Assays of Dkk-1 expression by MG63-Dkk1 cells
MG63-kdDkk1 and MG63-scr cells were cultured for 10 days under standard conditions. Dkk-1 secretion was measured in media supernatants by ELISA. Cells were counted by Cyquant fluorescent DNA quantification dye as previously described[104]. Messenger RNA and cDNA was synthesized using commercial kits (High Pure Kit, Roche Diagnostics, Indianapolis, IN and Superscript III Kit, Life Technologies respectively). Levels of cDNA encoding GAPDH (Hs02786624_g1) and Dkk-1 (Hs00183740_m1) were measured with Taq-Man primer and probe sets (Applied Biosystems, Waltham, MA) using a BioRad CFX96 Real-Time PCR System (BioRad, Hercules, CA, USA). Relative Dkk-1 expression between MG63-kdDkk1 and MG63-scr cells was determined using the $2^{-\Delta\Delta CT}$ method[108].

Enzyme linked immunosorbent assay (ELISA)
Cell conditioned media supernatants were stored at −20℃. For assays, they were thawed on ice thendiluted with phosphate buffered saline (PBS) containing 0.05% (v/v) Tween-20 (Millipore-Sigma) and 1% (w/v) bovine serum albumin (BSA) (Millipore-Sigma). Human Dkk-1 and OPG sandwich ELISAs were performed using the standard procedure recommended by the manufacturer (Duoset ELISA, R&D).

Immunoblotting
All electrophoresis, transfer and blotting was performed using Invitrogen (Watham, MA) XCell apparatus and reagents. Cell lysates were treated protease and phosphorylase inhibitors and were separated on 4–20% bis–tris gels using MES running buffer and transferred to PVDF membrane using tris–glycine transfer buffer. Blots were blocked in PBS containing 0.05% (v/v) Tween20 and 5% (w/v) dried milk (Millipore-Sigma) for 15 h. Primary antibodies were incubated for 4–15 h in PBS-T containing dried milk or 5% (w/v) BSA if probing for phosphorylated targets. The following antibodies were used in this study: anti-pJNK (#9255 at 1:500) and JNK (#9252 at 1:500–1:1000) (Cell Signaling Technologies, Boston, MA), anti-ALDH1A1 (ab134188 at 1:1000) (Abcam, Waltham, MA), GAPDH (ab8245 at 1: 2000) (Abcam), RhoA (#2177 at 1:500) (Cell Signaling Technologies), pMKK-4 (#9156 at 1:500) and MKK4 (#9152 at 1:500) (Cell Signaling Technologies), p-p38 (#4511 at 1:500) and p38 (#9212 at 1:500) (Cell Signaling Technologies).

Alkaline phosphatase and mineralization assays
Alkaline phosphatase assays were performed on monolayers or cell laden microcarriers using a spectrophotometric p-nitrophenyl-phosphate (PNPP) assay as previously described[82,104]. Data were expressed in terms of rate of substrate conversion normalized to cell number. Monolayer mineralization was measured by acid-mediated extraction of alizarin red S (ARS) from stained plates as described previously[104].

MOSJ-Dkk1-based assays
The purpose of these experiments was to examine how selected agents might perturb activity of the Dkk-1 activated PCP/ncWnt like pathway that drives ALDH1A1 expression. Because natural Dkk-1 expression (as seen in e.g. MG63 cells) can be affected by several parameters, it would be impossible to determine whether observed reductions in ALDH1A1 were a result of direct perturbation of the pathway, or were caused indirectly through variation in levels of Dkk-1 secretion. To solve this issue, we capitalized on the observation that parental MOSJ cells express marginal levels of Dkk-1 even under conditions of stress or when undergoing proliferation. In MOSJ-Dkk1 cells, Dkk-1 expression is achieved by an exogenous construct driven by a constitutive promoter
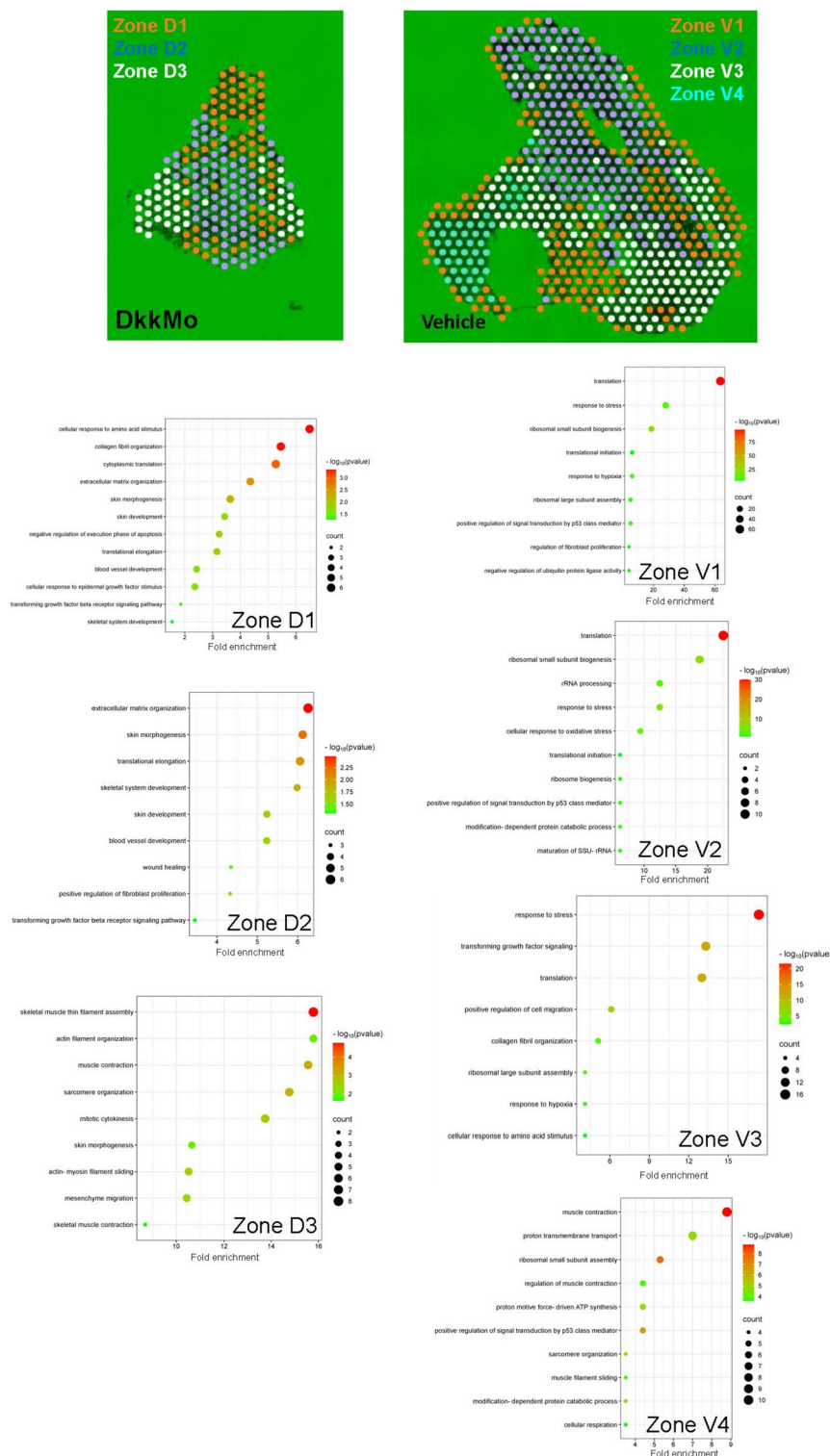
Fig. 7. Spatial distribution of gene signatures in a murine orthotopic model of human OS in presence or absence of DkkMo. Representative spatial gene expression analyses of DkkMo treated (left) and vehicle treated (right) tumor sections. Gene expression signatures cluster in three zones for DkkMo and four zones for vehicle treated tumors. Bubble plots of gene ontologies associated with each zone are presented under each section.

and there is a reduced likelihood that Dkk-1 output might be variable due to stress, proliferation rate or cell density. Using these cells provides a better read on the effects of the test agents on the PCP-like/ncWnt pathway rather than upstream perturbations of Dkk-1 expression caused by confounding factors.

MOSJ-Dkk1 cells[9] were plated in six-well format at 4000 cells per cm² in αMEM containing 10% (v/v) FBS and antibiotics. After 48 h, cells were incubated in the presence of inhibitors (Table 1) for a further 48 h followed by recovery of cells for quantitative qRT-PCR assays. Messenger RNA and cDNA synthesized using commercial kits (High Pure Kit, Roche Diagnostics, Indianapolis, IN and Superscript III Kit, Life Technologies respectively). Levels of cDNA encoding GAPDH (Mm99999915_g1) and ALDH1A1 (Mm00657317_m1) were measured with Taq-Man primer and probe sets (Applied Biosystems, Waltham, MA) using an ARIAMX Real-Time PCR System (Agilent Technologies, Santa Clara, CA, USA). Cells were enumerated by comparison of murine GAPDH levels to known standards and ALDH1A1 was determined using the $2^{-\Delta\Delta CT}$ method with normalization to GAPDH[108].

RWV-based assays

These experiments were performed as previously described[40] with some modifications. MG63 OS cells (1000 cells per cm⁻²) were fluorescently labeled with dsRed-tomato by transformation with lentiviral particles harboring the rLV-EF1a-tdTomato-IRES-Puro-WPR construct at a MOI of 10 in the presence of 9 µg.mL⁻¹ polybrene (Sigma). Transduced cells were selected in 9 µg.mL⁻¹ puromycin for 7 days then further purified by fluorescent activated cell sorting (FACS) (BDFACS Aria III, Texas A&M School of Medicine Cell Analysis Core). Human bone marrow-derived MSCs were labeled with GFP using lentiviral particles harboring the LV-EF1a-ZsGreen1-IRES-Puro-WPR construct at 2500 cells.cm⁻², MOI of 10, with pre-selection in 5 mg.mL⁻¹ puromycin followed by purification by FACS. Labeled cell preparations were then cultured under standard conditions to attain 50 million cells for cryopreservation as previously described[40]. For co-culture experiments, 2×10^5 GFP-hMSCs were mixed with 150 mg collagen I-coated polystyrene microcarriers (Corning, NY) in osteogenic base medium (OBM) consisting of alpha-minimal-essential-medium supplemented with 10% (v/v) FBS, 100 U.mL⁻¹ penicillin & 100 µg.mL⁻¹ streptomycin and 2 mM ʟ-glutamine, 50 mg.mL⁻¹ ascorbic acid (Sigma, St Louis, MO) and 5 mM β-glycerophosphate (Sigma). The suspension (10 mL) was loaded into a 10 mL capacity disposable high aspect ratio vessel (HARV) and 8 such cultures were fitted to a Synthecon RCCS-8DQ bioreactor (Synthecon, Houston, TX). After 48 h, a further 50,000 of dsRed labeled MG63 cells attached to collagen I spheres were added by replacement of 2.5 mL of medium after settling the hMSC-laden microcarriers. Rotation of the RWV was set to 12 rpm initially and adjusted daily to maintain freefall. Every 2 days, 7.5 mL of the medium was replaced with supplementation of experimental agents after settling of the microcarriers. Experiments were maintained 4 days. Cells were quantified while attached to microcarriers by direct fluorescent measurement and comparison with known standards (Fluostar Omega, BMG Labtech, Cary, NC). OPG:Dkk-1 ratios were calculated from ELISA measurements on media supernatants. ALP activity was measured on cell laden microcarriers using a PNPP colorimetric conversion assay described previously[82]. ALDH1A1 transcription was measured by qRT-PCR assay and normalized to GAPDH levels. For experiments involving PDX tumors, 500 mg tumor morsels were cultured in 10 mL HARVs for a total of 8 days in the presence of 10 µM DkkMo or scrMo. Masses and medium Dkk-1 levels were measured every 2 days. Glucose consumption was measured in media supernatants using a commercial glucose reader (Clarity Diagnostics, Boca Raton, FL).

Orthotopic OS model

All procedures described below are in accordance with an animal use protocol approved by the Texas A&M Institutional Animal Care and Use Committee and in accordance with ARRIVE guidelines. The PDX OS specimen DAR was used for this study[42]. Cryopreserved specimens of PDX were originally propagated as 30 mm³ subcutaneous implants on the flanks of NOD.Cg-Prkdc-SCID-IL2Rγ-null-tm1Wjl/SzJ (NSG mice, Jackson Laboratory) mice using Matrigel as a growth promoter[42]. When the tumors reached 10 mm in diameter (10–15 days), they were excised, morselized and slowly frozen in freezing medium containing phenol red-free α-MEM, 30% (v/v) FBS and 5% (v/v) dimethyl sulphoxide to −80 °C followed by storage in the vapor phase of liquid nitrogen. For establishment of the orthotopic OS model, 2-month-old NSG mice (five males, five females) were maintained under isoflurane (Sigma) anesthesia while the left hindlimb was shaved and sanitized. A 1.5 cm incision was made on the medial side of the hindlimb and the femur was exposed by dissecting below the *vastus lateralis* muscle. Tissue was separated from the surface of the femur by blunt dissection and the periosteum of the diaphysis of the femur scraped with a scalpel. Approximately 30 mm³ of PDX was coated in Matrigel and implanted on the medial side of the femur at midpoint. Muscle and skin were closed by suture. After 1 week, treatment was initiated by intraperitoneal injection of DkkMo (12.5 mg.kg⁻¹) suspended in 100 µL of sterile PBS every 48 h[27]. Controls received vehicle. Every 2 days, hindlimbs were scanned by ultrasound (Vevo3100, Visual Sonics, Toronto, Canada) using the 550 probe with center frequency of 40 MHz to follow tumor expansion. At the conclusion of the study, mice were humanely euthanized by intraperitoneal administration of Euthasol (Virbac, Westlake, TX) under isoflurane anesthesia.

Microtomographic (µCT) imaging of PDX tumors

Hindlimbs were dissected by intact release of the femoral head from the acetabulum. Skinned hindlimbs were fixed for 1 week in phosphate buffered formalin (PBF) at 4 °C. Scans were performed using a Skyscan1275 Microtomograph (Bruker, Billerica, MA) as previously described[27]. A filtered (1.5 mm aluminum) beam was set to 40 kV, 250 µA and image capture set to 11 µm resolution. Smoothing and beam hardening was set to 2% (smoothing kernel gaussian) and 25%, respectively. Axial reconstructions were performed using NRecon software (Bruker), generating 30 µm-thick slices at 12 µm resolution. Ring artifact reduction and misalignment correction were adjusted manually. The dynamic range was set to between −1000 and 7519.5 HU for reconstructions. Specimens were then contrast stained with Lugol's iodine/potassium iodide (IKI) for two weeks[109], then rescanned to facilitate detection of soft tissues and tumors.

Measurement of tumor volume and bone parameters

Femur reconstructions were vertically oriented and the distance was measured from the proximal extent of the greater trochanter to the midpoint between the lateral and medial condyles. Using these measurements, the central 1/3 of the femur encompassing the contact region between tumor and diaphysis was selected as the primary region of interest (ROI) for measurements. Standard osteomorphometric and volumetric calculations were performed on 3D ROIs using CT*Anal* software (Bruker). Tumor volume measurements were achieved by manual and semi-automated demarcation of the tumor margins on axial reconstructions using CT*Anal* software.

Quantification and visualization of PDX tumor necrosis

Two parallel biopsies were extracted from 8 PDX tumors from each group using a 2 mm wide biopsy punch approximately 5 mm long (Fig. 5C). One biopsy from each sample was stored in 70% (v/v) ethanol for histology. The second biopsy was weighed and then DNA was extracted by affinity purification (DNeasy Kit, Qiagen, Redwood City, CA) and quantified by spectrophotometry (Nanodrop, ThermoFisher Scientific, Waltham, MA). Samples were incubated in decalcifying solution (Richard-Allan Scientific, San Diego, CA) until bone was radiolucent by μCT using the same parameters used for analysis. Tissue was processed, paraffin embedded, sectioned into 4 μm sections, and stained with hematoxylin and eosin by the Research Histology Unit at the Texas A&M University School of Veterinary and Biomedical Sciences.

Metastasis assays

RNA was extracted from flash frozen morselized mouse lungs with an initial lysis in RNeasy lysis buffer (Qiagen), prior to extrusion of lysates through a 28-gauge needle. Lysates were then processed by affinity purification (RNeasy Midi kit, Qiagen) in accordance with manufacturer's protocols. Pure RNA was precipitated with glycogen (Thermo Scientific) to a concentration of >50 μg.mL^{-1}. The SuperScript IV First-Strand Synthesis Kit (Invitrogen) was used for cDNA synthesis in accordance with the manufacturers protocol using random hexamers and oligo dT primers to prime 10 μL of the pure RNA solution. Quantitative RT-PCR was performed using 300 ng of cDNA with Fast SYBR Green Master Mix (Applied Biosystems, Thermo Fisher Scientific) according to the manufacturers protocols with a StepOnePlus Real-Time PCR System (Applied Biosystems, Thermo Fisher Scientific). Species specific human GAPDH primers (RTPrimerDB ID_1242): ctctctgctcctcctgttcgac (fwd) and tgagcgatgtggctcggct (rev) and mouse GAPDH primers (RTPrimerDB ID_473): catggccttccgtgttccta (fwd) and gcggcacgtcagatcca (rev) were used with a 50 °C annealing temperature.

Single cell RNA sequencing

Single cell suspensions of tumors and peripheral tissue were prepared in accordance with manufacturer protocols and sequenced on a 10× Chromium System (10× Genomics, Pleasanton, CA). Paired read files were uploaded to 10× Genomics Cloud Analysis and Cell Ranger Count v7.0.1 was used to align the data to the Human (GRCh38) 2020-A genome. The resulting filtered feature matrix files was then loaded into Seurat[110]. Control and treatment groups were assigned metadata for their respective groups and merged into a single Seurat object. Quality control was performed by filtering out cells with fewer than 200 RNA features. The proportion of mitochondrial and ribosomal genes expressed was assessed for additional filtration but no additional removal was necessary. The dataset was normalized and non-linear dimensional reduction (UMAP) was performed to plot gene expression clusters labeled by group, unique genes compared to other clusters, and cell cycle. Gene ontology term enrichment was visualized by use of the Database for Annotation, Visualization and Integrated Discovery (DAVID) website[111], GOnet (DICE Tools)[112,113] and SR Plot[114]. Tissue biomarker expression was evaluated for each cluster using PanglaoDB[115] and in the case of immune cells, confirmed by CellTypeScore (DICE Tools).

Spatial gene expression

Tumors were sectioned and mounted onto Visium slides (10× Genomics), imaged by fluorescence microscopy, and sequenced in accordance with manufacturer protocols on a Chromium system (10× Genomics). Paired read files and the red channel micrograph were used as inputs to SpaceRanger Count v.2.0.1 (10× Genomics) and aligned to the Human (GRCh38) 2020-A genome. Differentially expressed genes were analyzed using Loupe Browser (10× Genomics). Differentially expressed genes were analyzed using Genecards to determine a predominant function for each cluster.

Statistics

Statistics were calculated using GraphPad Prism version 5 and 10 (Dotmatics, Boston, MA) or by the software packages utilized for single cell sequencing analyses. Specific details regarding statistical analyses are provided in figure legends.

Data availability

Raw data available by contact with the corresponding author. Sequencing data submitted to the NCBI Sequence Read Archive, BioSample accessions: SAMN43382912 and SAMN43382913.

References

1. Ottaviani, G. & Jaffe, N. The epidemiology of osteosarcoma. *Cancer Treat. Res.* **152**, 3–13. https://doi.org/10.1007/978-1-4419-02 84-9_1 (2009).

2. Sheng, G., Gao, Y., Yang, Y. & Wu, H. Osteosarcoma and Metastasis. *Front. Oncol.* **11**, 780264. https://doi.org/10.3389/fonc.2021.780264 (2021).
3. Misaghi, A., Goldin, A., Awad, M. & Kulidjian, A. A. Osteosarcoma: a comprehensive review. *SICOT J.* **4**, 12. https://doi.org/10.1051/sicotj/2017028 (2018).
4. Isakoff, M. S., Bielack, S. S., Meltzer, P. & Gorlick, R. Osteosarcoma: Current treatment and a collaborative pathway to success. *J. Clin. Oncol.* **33**, 3029–3035. https://doi.org/10.1200/JCO.2014.59.4895 (2015).
5. Stiller, C. A., Craft, A. W. & Corazziari, I. Survival of children with bone sarcoma in Europe since 1978: results from the EUROCARE study. *Eur. J. Cancer* **37**, 760–766. https://doi.org/10.1016/s0959-8049(01)00004-1 (2001).
6. Sugito, W. & Kamal, A. F. Clinical outcome following prolonged neoadjuvant chemotherapy and delayed surgery in osteosarcoma patients: An evidence-based clinical review. *Acta Med. Indones* **54**, 142–150 (2022).
7. Rudnicki, M. A. & Williams, B. O. Wnt signaling in bone and muscle. *Bone* **80**, 60–66. https://doi.org/10.1016/j.bone.2015.02.009 (2015).
8. Tian, E. et al. The role of the Wnt-signaling antagonist DKK1 in the development of osteolytic lesions in multiple myeloma. *N. Engl. J. Med.* **349**, 2483–2494. https://doi.org/10.1056/NEJMoa030847349/26/2483 (2003).
9. Krause, U., Ryan, D. M., Clough, B. H. & Gregory, C. A. An unexpected role for a Wnt-inhibitor: Dickkopf-1 triggers a novel cancer survival mechanism through modulation of aldehyde-dehydrogenase-1 activity. *Cell Death Dis.* **5**, e1093. https://doi.org/10.1038/cddis.2014.67 (2014).
10. Arnulf, B. et al. Phenotypic and functional characterization of bone marrow mesenchymal stem cells derived from patients with multiple myeloma. *Leukemia* **21**, 158–163 (2007).
11. Corre, J. et al. Bone marrow mesenchymal stem cells are abnormal in multiple myeloma. *Leukemia* **21**, 1079–1088. https://doi.org/10.1038/sj.leu.2404621 (2007).
12. Gunn, W. G. et al. A crosstalk between myeloma cells and marrow stromal cells stimulates production of DKK1 and interleukin-6: a potential role in the development of lytic bone disease and tumor progression in multiple myeloma. *Stem Cells* **24**, 986–991. https://doi.org/10.1634/stemcells.2005-0220 (2006).
13. Fowler, J. A., Mundy, G. R., Lwin, S. T. & Edwards, C. M. Bone marrow stromal cells create a permissive microenvironment for myeloma development: a new stromal role for wnt inhibitor dkk1. *Cancer Res.* **72**, 2183–2189. https://doi.org/10.1158/0008-5472.CAN-11-2067 (2012).
14. Edwards, C. M. et al. Increasing Wnt signaling in the bone marrow microenvironment inhibits the development of myeloma bone disease and reduces tumor burden in bone in vivo. *Blood* **111**, 2833–2842. https://doi.org/10.1182/blood-2007-03-077685 (2008).
15. Garderet, L. et al. Mesenchymal stem cell abnormalities in patients with multiple myeloma. *Leuk. Lymphoma* **48**, 2032–2041. https://doi.org/10.1080/10428190701593644 (2007).
16. Saad, F. et al. Pathologic fractures correlate with reduced survival in patients with malignant bone disease. *Cancer* **110**, 1860–1867. https://doi.org/10.1002/cncr.22991 (2007).
17. Thudi, N. K. et al. Dickkopf-1 (DKK-1) stimulated prostate cancer growth and metastasis and inhibited bone formation in osteoblastic bone metastases. *Prostate* **71**, 615–625. https://doi.org/10.1002/pros.21277 (2011).
18. Supsavhad, W. et al. Effect of Dickkopf-1 (Dkk-1) and SP600125, a JNK inhibitor, on Wnt signaling in canine prostate cancer growth and bone metastases. *Vet. Sci.* https://doi.org/10.3390/vetsci8080153 (2021).
19. Makia, N. L., Bojang, P., Falkner, K. C., Conklin, D. J. & Prough, R. A. Murine hepatic aldehyde dehydrogenase 1a1 is a major contributor to oxidation of aldehydes formed by lipid peroxidation. *Chem. Biol. Interact.* **191**, 278–287. https://doi.org/10.1016/j.cbi.2011.01.013 (2011).
20. Awad, O. et al. High ALDH activity identifies chemotherapy-resistant Ewing's sarcoma stem cells that retain sensitivity to EWS-FLI1 inhibition. *PLoS One* **5**, e13943. https://doi.org/10.1371/journal.pone.0013943 (2010).
21. Honoki, K. et al. Possible involvement of stem-like populations with elevated ALDH1 in sarcomas for chemotherapeutic drug resistance. *Oncol. Rep.* **24**, 501–505 (2010).
22. Kim, R. J. et al. High aldehyde dehydrogenase activity enhances stem cell features in breast cancer cells by activating hypoxia-inducible factor-2alpha. *Cancer Lett.* **333**, 18–31. https://doi.org/10.1016/j.canlet.2012.11.026 (2013).
23. Greco, N. et al. ALDH activity correlates with metastatic potential in primary sarcomas of bone. *J. Cancer Ther.* **5**, 331–338. https://doi.org/10.4236/jct.2014.54040 (2014).
24. Martinez-Cruzado, L. et al. Aldh1 expression and activity increase during tumor evolution in sarcoma cancer stem cell populations. *Sci. Rep.* **6**, 27878. https://doi.org/10.1038/srep27878 (2016).
25. Douville, J., Beaulieu, R. & Balicki, D. ALDH1 as a functional marker of cancer stem and progenitor cells. *Stem Cells Dev.* **18**, 17–25. https://doi.org/10.1089/scd.2008.0055 (2009).
26. Rodriguez-Torres, M. & Allan, A. L. Aldehyde dehydrogenase as a marker and functional mediator of metastasis in solid tumors. *Clin. Exp. Metastasis* **33**, 97–113. https://doi.org/10.1007/s10585-015-9755-9 (2016).
27. Pan, S. et al. Morpholino-driven blockade of Dkk-1 in osteosarcoma inhibits bone damage and tumour expansion by multiple mechanisms. *Br. J. Cancer* https://doi.org/10.1038/s41416-022-01764-z (2022).
28. Lee, N. et al. A potential role for Dkk-1 in the pathogenesis of osteosarcoma predicts novel diagnostic and treatment strategies. *Br. J. Cancer* **97**, 1552–1559. https://doi.org/10.1038/sj.bjc.6604069 (2007).
29. Gregory, C. A., Singh, H., Perry, A. S. & Prockop, D. J. The Wnt signaling inhibitor dickkopf-1 is required for reentry into the cell cycle of human adult stem cells from bone marrow. *J. Biol. Chem.* **278**, 28067–28078 (2003).
30. Nicoletto, R. E. & Ofner, C. M. 3rd. Cytotoxic mechanisms of doxorubicin at clinically relevant concentrations in breast cancer cells. *Cancer Chemother. Pharmacol.* **89**, 285–311. https://doi.org/10.1007/s00280-022-04400-y (2022).
31. Gregory, C. A. et al. How Wnt signaling affects bone repair by mesenchymal stem cells from the bone marrow. *Ann. N. Y. Acad. Sci.* **1049**, 97–106. https://doi.org/10.1196/annals.1334.010 (2005).
32. Gregory, C. A. et al. Dkk-1-derived synthetic peptides and lithium chloride for the control and recovery of adult stem cells from bone marrow. *J. Biol. Chem.* **280**, 2309–2323. https://doi.org/10.1074/jbc.M406275200 (2005).
33. Krause, U. et al. Pharmaceutical modulation of canonical Wnt signaling in multipotent stromal cells for improved osteoinductive therapy. *Proc. Natl. Acad. Sci. U. S. A.* **107**, 4147–4152. https://doi.org/10.1073/pnas.0914360107 (2010).
34. Krause, U. & Gregory, C. A. Potential of modulating Wnt signaling pathway toward the development of bone anabolic agent. *Curr. Mol. Pharmacol.* **5**(2), 164–173 (2011).
35. Makia, N. L. et al. AP-1 regulation of murine aldehyde dehydrogenase 1a1. *Mol. Pharmacol.* https://doi.org/10.1124/mol.112.078147 (2012).
36. Lawson, C. D. & Burridge, K. The on-off relationship of Rho and Rac during integrin-mediated adhesion and cell migration. *Small GTPases* **5**, e27958. https://doi.org/10.4161/sgtp.27958 (2014).
37. Iyer, S. P. et al. A Phase IB multicentre dose-determination study of BHQ880 in combination with anti-myeloma therapy and zoledronic acid in patients with relapsed or refractory multiple myeloma and prior skeletal-related events. *Br. J. Haematol.* **167**, 366–375. https://doi.org/10.1111/bjh.13056 (2014).
38. Fulciniti, M. et al. Anti-DKK1 mAb (BHQ880) as a potential therapeutic agent for multiple myeloma. *Blood* **114**, 371–379. https://doi.org/10.1182/blood-2008-11-191577 (2009).
39. Yaccoby, S. et al. Antibody-based inhibition of DKK1 suppresses tumor-induced bone resorption and multiple myeloma growth in vivo. *Blood* **109**, 2106–2111 (2007).

20

40. McNeill, E. P. et al. Characterization of a pluripotent stem cell-derived matrix with powerful osteoregenerative capabilities. *Nat. Commun.* **11**, 3025. https://doi.org/10.1038/s41467-020-16646-2 (2020).
41. Goldstein, S. D., Trucco, M., Guzman, W. B., Hayashi, M. & Loeb, D. M. A monoclonal antibody against the Wnt signaling inhibitor dickkopf-1 inhibits osteosarcoma metastasis in a preclinical model. *Oncotarget* https://doi.org/10.18632/oncotarget.8522 (2016).
42. Goldstein, S. D., Hayashi, M., Albert, C. M., Jackson, K. W. & Loeb, D. M. An orthotopic xenograft model with survival hindlimb amputation allows investigation of the effect of tumor microenvironment on sarcoma metastasis. *Clin. Exp. Metastasis* **32**, 703–715. https://doi.org/10.1007/s10585-015-9738-x (2015).
43. Doucet, D., Brubaker, C., Turner, D. & Gregory, C. A. Factors affecting the role of canonical Wnt inhibitor Dickkopf-1 in cancer progression. *Front. Oncol.* **13**, 1114822. https://doi.org/10.3389/fonc.2023.1114822 (2023).
44. Meijer, L. et al. GSK-3-selective inhibitors derived from Tyrian purple indirubins. *Chem. Biol.*, **10**, 1255–1266,https://doi.org/10.1016/j.chembiol.2003.11.010 (2003).
45. Ewan, K. et al. A useful approach to identify novel small-molecule inhibitors of Wnt-dependent transcription.*Cancer. Res.* **70**, 5963–5973, https://doi.org/10.1158/0008-5472.CAN-10-1028 (2010).
46. Benink, H. A. & Bement, W. M. Concentric zones of active RhoA and Cdc42 around single cell wounds. *J. Cell. Biol.* **168**, 429–439, https://doi.org/10.1083/jcb.200411109 (2005).
47. Ruocco, K. M. et al. A high-throughput cell-based assay to identify specific inhibitors of transcription factor AP-1. *J. Biomol. Screen.* **12**, 133–139, https://doi.org/10.1177/1087057106296686 (2007).
48. Gao, Y., Dickerson, J. B., Guo, F., Zheng, J. & Zheng, Y. Rational design and characterization of a Rac GTPasespecific small molecule inhibitor. *Proc. Natl. Acad. Sci. U S A* **101**, 7618–7623, https://doi.org/10.1073/pnas.0307512101 (2004).
49. Cuenda, A. et al. SB 203580 is a specific inhibitor of a MAP kinase homologue which is stimulated by cellular stresses and interleukin-1. *FEBS Lett* **364**, 229–233 (1995).
50. Bennett, B. L. et al. SP600125, an anthrapyrazolone inhibitor of Jun N-terminal kinase. *Proc. Natl. Acad. Sci. U S A* **98**, 13681–13686, https://doi.org/10.1073/pnas.251194298 (2001).
51. Fedi, P. et al. Isolation and biochemical characterization of the human Dkk-1 homologue, a novel inhibitor of mammalian Wnt signaling. *J. Biol. Chem.* **274**, 19465–19472. https://doi.org/10.1074/jbc.274.27.19465 (1999).
52. Chidiac, R. & Angers, S. Wnt signaling in stem cells during development and cell lineage specification. *Curr. Top. Dev. Biol.* **153**, 121–143. https://doi.org/10.1016/bs.ctdb.2023.01.005 (2023).
53. Hayat, R., Manzoor, M. & Hussain, A. Wnt signaling pathway: A comprehensive review. *Cell Biol. Int.* **46**, 863–877. https://doi.org/10.1002/cbin.11797 (2022).
54. Wen, X., Wu, Y., Awadasseid, A., Tanaka, Y. & Zhang, W. New advances in canonical Wnt/beta-catenin signaling in cancer. *Cancer Manag. Res.* **12**, 6987–6998. https://doi.org/10.2147/CMAR.S258645 (2020).
55. Cai, Y., Cai, T. & Chen, Y. Wnt pathway in osteosarcoma, from oncogenic to therapeutic. *J. Cell Biochem.* **115**, 625–631. https://doi.org/10.1002/jcb.24708 (2014).
56. Iwaya, K. et al. Cytoplasmic and/or nuclear staining of beta-catenin is associated with lung metastasis. *Clin. Exp. Metastasis* **20**, 525–529. https://doi.org/10.1023/a:1025821229013 (2003).
57. Haydon, R. C. et al. Cytoplasmic and/or nuclear accumulation of the beta-catenin protein is a frequent event in human osteosarcoma. *Int. J. Cancer* **102**, 338–342. https://doi.org/10.1002/ijc.10719 (2002).
58. Cai, W., Xu, Y., Yin, J., Zuo, W. & Su, Z. miR-552-5p facilitates osteosarcoma cell proliferation and metastasis by targeting WIF1. *Exp. Ther. Med.* **17**, 3781–3788. https://doi.org/10.3892/etm.2019.7361 (2019).
59. Kansara, M. et al. Wnt inhibitory factor 1 is epigenetically silenced in human osteosarcoma, and targeted disruption accelerates osteosarcomagenesis in mice. *J. Clin. Investig.* **119**, 837–851. https://doi.org/10.1172/JCI37175 (2009).
60. Han, W. & Liu, J. Epigenetic silencing of the Wnt antagonist APCDD1 by promoter DNA hyper-methylation contributes to osteosarcoma cell invasion and metastasis. *Biochem. Biophys. Res. Commun.* **491**, 91–97. https://doi.org/10.1016/j.bbrc.2017.07.049 (2017).
61. Singla, A. et al. Wnt signaling in osteosarcoma. *Adv. Exp. Med. Biol.* **1258**, 125–139. https://doi.org/10.1007/978-3-030-43085-6_8 (2020).
62. Danieau, G. et al. ICG-001, an inhibitor of the beta-catenin and cAMP response element-binding protein dependent gene transcription, decreases proliferation but enhances migration of osteosarcoma cells. *Pharmaceuticals* https://doi.org/10.3390/ph14050421 (2021).
63. Zhao, S. J. et al. SPARCL1 suppresses osteosarcoma metastasis and recruits macrophages by activation of canonical WNT/beta-catenin signaling through stabilization of the WNT-receptor complex. *Oncogene* **37**, 1049–1061. https://doi.org/10.1038/onc.2017.403 (2018).
64. Cai, Y. et al. Inactive Wnt/beta-catenin pathway in conventional high-grade osteosarcoma. *J. Pathol.* **220**, 24–33. https://doi.org/10.1002/path.2628 (2010).
65. Fezza, M., Moussa, M., Aoun, R., Haber, R. & Hilal, G. DKK1 promotes hepatocellular carcinoma inflammation, migration and invasion: Implication of TGF-beta1. *PLoS One* **14**, e0223252. https://doi.org/10.1371/journal.pone.0223252 (2019).
66. Matushansky, I. et al. Derivation of sarcomas from mesenchymal stem cells via inactivation of the Wnt pathway. *J. Clin. Investig.* **117**, 3248–3257. https://doi.org/10.1172/JCI31377 (2007).
67. Pan, T. C. et al. A mouse model for dominant collagen VI disorders: heterozygous deletion of Col6a3 Exon 16. *J. Biol. Chem.* **289**, 10293–10307. https://doi.org/10.1074/jbc.M114.549311 (2014).
68. Kikuchi, A., Fumoto, K. & Kimura, H. The Dickkopf1-cytoskeleton-associated protein 4 axis creates a novel signalling pathway and may represent a molecular target for cancer therapy. *Br. J. Pharmacol.* **174**, 4651–4665. https://doi.org/10.1111/bph.13863 (2017).
69. Li, X. et al. DKK1 activates noncanonical NF-kappaB signaling via IL-6-induced CKAP4 receptor in multiple myeloma. *Blood Adv.* **5**, 3656–3667. https://doi.org/10.1182/bloodadvances.2021004315 (2021).
70. Bhavanasi, D., Speer, K. F. & Klein, P. S. CKAP4 is identified as a receptor for Dickkopf in cancer cells. *J. Clin. Investig.* **126**, 2419–2421. https://doi.org/10.1172/JCI88620 (2016).
71. Suchitha, G. P., Balaya, R. D. A., Raju, R., Keshava Prasad, T. S. & Dagamajalu, S. A network map of cytoskeleton-associated protein 4 (CKAP4) mediated signaling pathway in cancer. *J. Cell Commun. Signal.* **17**, 1097–1104. https://doi.org/10.1007/s12079-023-00739-w (2023).
72. Khamidullina, A. I., Abramenko, Y. E., Bruter, A. V. & Tatarskiy, V. V. Key proteins of replication stress response and cell cycle control as cancer therapy targets. *Int. J. Mol. Sci.* https://doi.org/10.3390/ijms25021263 (2024).
73. Techer, H., Koundrioukoff, S., Nicolas, A. & Debatisse, M. The impact of replication stress on replication dynamics and DNA damage in vertebrate cells. *Nat. Rev. Genet.* **18**, 535–550. https://doi.org/10.1038/nrg.2017.46 (2017).
74. Prockop, D. J., Gregory, C. A. & Spees, J. L. One strategy for cell and gene therapy: harnessing the power of adult stem cells to repair tissues. *Proc. Natl. Acad. Sci. U. S. A.* **100**(Suppl 1), 11917–11923. https://doi.org/10.1073/pnas.1834138100[pii] (2003).
75. Marchitti, S. A., Brocker, C., Stagos, D. & Vasiliou, V. Non-P450 aldehyde oxidizing enzymes: the aldehyde dehydrogenase superfamily. *Expert Opin. Drug Metab. Toxicol.* **4**, 697–720. https://doi.org/10.1517/17425255.4.6.697 (2008).
76. Meng, E. et al. ALDH1A1 maintains ovarian cancer stem cell-like properties by altered regulation of cell cycle checkpoint and DNA repair network signaling. *PLoS One* **9**, e107142. https://doi.org/10.1371/journal.pone.0107142 (2014).

77. Marina, N. M. et al. Comparison of MAPIE versus MAP in patients with a poor response to preoperative chemotherapy for newly diagnosed high-grade osteosarcoma (EURAMOS-1): an open-label, international, randomised controlled trial. *Lancet Oncol.* **17**, 1396–1408. https://doi.org/10.1016/S1470-2045(16)30214-5 (2016).

78. Shou, J. et al. Human Dkk-1, a gene encoding a Wnt antagonist, responds to DNA damage and its overexpression sensitizes brain tumor cells to apoptosis following alkylation damage of DNA. *Oncogene* **21**, 878–889. https://doi.org/10.1038/sj.onc.1205138 (2002).

79. Hare, I. et al. Chemotherapy-induced Dkk-1 expression by primary human mesenchymal stem cells is p53 dependent. *Med. Oncol.* **33**, 113. https://doi.org/10.1007/s12032-016-0826-9 (2016).

80. Wise, D. R. et al. A phase 1/2 multicenter trial of DKN-01 as monotherapy or in combination with docetaxel for the treatment of metastatic castration-resistant prostate cancer (mCRPC). *Prostate Cancer Prostatic Dis.* https://doi.org/10.1038/s41391-024-00798-z (2024).

81. Arend, R. et al. DKK1 is a predictive biomarker for response to DKN-01: Results of a phase 2 basket study in women with recurrent endometrial carcinoma. *Gynecol. Oncol.* **172**, 82–91. https://doi.org/10.1016/j.ygyno.2023.03.013 (2023).

82. McNeill, E. P. et al. Three-dimensional in vitro modeling of malignant bone disease recapitulates experimentally accessible mechanisms of osteoinhibition. *Cell Death Dis.* **9**, 1161. https://doi.org/10.1038/s41419-018-1203-8 (2018).

83. Perivoliotis, K. et al. Microvessel density (MVD) in patients with osteosarcoma: A systematic review and meta-analysis. *Cancer Investig.* **42**, 104–114. https://doi.org/10.1080/07357907.2024.2311266 (2024).

84. Griffith, C. K. et al. Diffusion limits of an in vitro thick prevascularized tissue. *Tissue Eng.* **11**, 257–266. https://doi.org/10.1089/ten.2005.11.257 (2005).

85. Morcos, P. A., Li, Y. & Jiang, S. Vivo-morpholinos: a non-peptide transporter delivers morpholinos into a wide array of mouse tissues. *BioTechniques* **45**, 613–614 (2008).

86. Ho Shon, I. & Hogg, P. J. Imaging of cell death in malignancy: Targeting pathways or phenotypes?. *Nucl. Med. Biol.* **124–125**, 108380. https://doi.org/10.1016/j.nucmedbio.2023.108380 (2023).

87. Mandell, J. B. et al. ALDH1A1 gene expression and cellular copper levels between low and highly metastatic osteosarcoma provide a case for novel repurposing with disulfiram and copper. *Sarcoma* **2022**, 7157507. https://doi.org/10.1155/2022/7157507 (2022).

88. Yuan, J. et al. Long intergenic non-coding RNA DIO3OS promotes osteosarcoma metastasis via activation of the TGF-beta signaling pathway: a potential diagnostic and immunotherapeutic target for osteosarcoma. *Cancer Cell Int.* **23**, 215. https://doi.org/10.1186/s12935-023-03076-5 (2023).

89. Liu, Y. et al. Logistic regression analysis for the identification of the metastasis-associated signaling pathways of osteosarcoma. *Int. J. Mol. Med.* **41**, 1233–1244. https://doi.org/10.3892/ijmm.2018.3360 (2018).

90. Shultz, L. D. et al. Human lymphoid and myeloid cell development in NOD/LtSz-scid IL2R gamma null mice engrafted with mobilized human hemopoietic stem cells. *J. Immunol.* **174**, 6477–6489. https://doi.org/10.4049/jimmunol.174.10.6477 (2005).

91. Behan, J. W. et al. Activation of adipose tissue macrophages in obese mice does not require lymphocytes. *Obesity* **21**, 1380–1388. https://doi.org/10.1002/oby.20159 (2013).

92. Zhou, Q., Facciponte, J., Jin, M., Shen, Q. & Lin, Q. Humanized NOD-SCID IL2rg-/- mice as a preclinical model for cancer research and its potential use for individualized cancer therapies. *Cancer Lett.* **344**, 13–19. https://doi.org/10.1016/j.canlet.2013.10.015 (2014).

93. Jaschke, N. P. et al. Dickkopf1 fuels inflammatory cytokine responses. *Commun. Biol.* **5**, 1391. https://doi.org/10.1038/s42003-022-04368-8 (2022).

94. Guo, Y. et al. Platelet-derived Wnt antagonist Dickkopf-1 is implicated in ICAM-1/VCAM-1-mediated neutrophilic acute lung inflammation. *Blood* **126**, 2220–2229. https://doi.org/10.1182/blood-2015-02-622233 (2015).

95. Giordano, P. et al. High Dickkopf-1 levels are associated with chronic inflammation in children with sickle cell disease. *Eur. J. Haematol.* **108**, 336–341. https://doi.org/10.1111/ejh.13741 (2022).

96. Kim, M. J. & Choe, Y. H. Correlation of Dickkopf-1 with inflammation in crohn disease. *Indian Pediatr.* **56**, 929–932 (2019).

97. Song, X. et al. Systemic inflammatory markers for predicting overall survival in patients with osteosarcoma: A systematic review and meta-analysis. *Mediat. Inflamm.* **2021**, 3456629. https://doi.org/10.1155/2021/3456629 (2021).

98. Wang, X., Wu, Z., Zhang, Z. & Jiang, Z. Prognostic and clinicopathological value of systemic immune-inflammation index in patients with osteosarcoma: a meta-analysis. *Front. Immunol.* **15**, 1416068. https://doi.org/10.3389/fimmu.2024.1416068 (2024).

99. He, X. et al. Prognostic significance of modified lung immune prognostic index in osteosarcoma patients. *Front. Genet.* **13**, 972352. https://doi.org/10.3389/fgene.2022.972352 (2022).

100. Liu, B. et al. Prognostic value of inflammation-based scores in patients with osteosarcoma. *Sci. Rep.* **6**, 39862. https://doi.org/10.1038/srep39862 (2016).

101. Jaschke, N., Hofbauer, L. C., Gobel, A. & Rachner, T. D. Evolving functions of Dickkopf-1 in cancer and immunity. *Cancer Lett.* **482**, 1–7. https://doi.org/10.1016/j.canlet.2020.03.031 (2020).

102. Russinoff, S., Miran, S., Gowda, A. L. & Lucas, P. A. Osteosarcoma cells differentiate into phenotypes from all three dermal layers. *Clin. Orthop. Relat. Res.* **469**, 2895–2904. https://doi.org/10.1007/s11999-011-1946-3 (2011).

103. Yu, L., Guo, W., Zhao, S., Wang, F. & Xu, Y. Fusion between cancer cells and myofibroblasts is involved in osteosarcoma. *Oncol. Lett.* **2**, 1083–1087. https://doi.org/10.3892/ol.2011.363 (2011).

104. Krause, U., Seckinger, A. & Gregory, C. A. Assays of osteogenic differentiation by cultured human mesenchymal stem cells. *Methods Mol. Biol.* **698**, 215–230. https://doi.org/10.1007/978-1-60761-999-4_17 (2011).

105. Gunn, W. G., Krause, U., Lee, N. & Gregory, C. A. Pharmaceutical inhibition of glycogen synthetase kinase-3beta reduces multiple myeloma-induced bone disease in a novel murine plasmacytoma xenograft model. *Blood* **117**, 1641–1651. https://doi.org/10.1182/blood-2010-09-308171 (2011).

106. Li, J. et al. The synergistic anticancer effect of CBD and DOX in osteosarcoma. *Clin. Transl. Oncol.* **25**, 2408–2418. https://doi.org/10.1007/s12094-023-03119-3 (2023).

107. She, F. et al. Melatonin protects MG63 osteoblast-like cells from hydrogen peroxide-induced cytotoxicity by maintaining mitochondrial function. *Mol. Med. Rep.* **9**, 493–498. https://doi.org/10.3892/mmr.2013.1832 (2014).

108. Livak, K. J. & Schmittgen, T. D. Analysis of relative gene expression data using real-time quantitative PCR and the 2(-delta delta C(T)) method. *Methods* **25**, 402–408 (2001).

109. Metscher, B. D. MicroCT for comparative morphology: simple staining methods allow high-contrast 3D imaging of diverse non-mineralized animal tissues. *BMC Physiol.* **9**, 11. https://doi.org/10.1186/1472-6793-9-11 (2009).

110. Hao, Y. et al. Dictionary learning for integrative, multimodal and scalable single-cell analysis. *Nat. Biotechnol.* https://doi.org/10.1038/s41587-023-01767-y (2023).

111. Dennis, G. et al. DAVID: Database for annotation, visualization, and integrated discovery. *Genome Biol.* **4**, P3 (2003).

112. Chandra, V. et al. Promoter-interacting expression quantitative trait loci are enriched for functional genetic variants. *Nat. Genet.* **53**, 110–119. https://doi.org/10.1038/s41588-020-00745-3 (2021).

113. Schmiedel, B. J. et al. Impact of genetic polymorphisms on human immune cell gene expression. *Cell* **175**, 1701–1715. https://doi.org/10.1016/j.cell.2018.10.022 (2018).

114. Tang, D. et al. SRplot: A free online platform for data visualization and graphing. *PLoS One* **18**, e0294236. https://doi.org/10.1371/journal.pone.0294236 (2023).

115. Franzen, O., Gan, L. M. & Bjorkegren, J. L. M. PanglaoDB: a web server for exploration of mouse and human single-cell RNA sequencing data. *Database* https://doi.org/10.1093/database/baz046 (2019).

Acknowledgements

Author contributions

Conceptualization, A.H., S.P, R.K., and C.A.G.; methodology, A.H., S.P., R.R., A.P., R.K., and C.A.G.; formal analysis, A.H., J.C.B.; investigation, A.H., S.P., R.R., A.P., M.G.L., S.L., C.S., and J.B.; resources, A.H., S.P., R.K., and C.A.G.; writing—original draft, A.H., S.P., M.G.L., S.L., C.S., J.B., and C.A.G; writing—review and editing, all authors; supervision, R.K. and C.A.G.; project administration, A.H., S.P., R.K., and C.A.G.; funding acquisition, R.K. and C.A.G.

Declarations

Competing interests

The authors declare no competing interests.

Ethics approval

Animal studies were performed in accordance with a protocol approved by the Texas A&M Animal Care and Use Committee and in accordance with ARRIVE guidelines (ARRIVE checklist attached). The work described herein did not involve human subjects as defined by the National Institutes of Health guidelines.

Additional information

Supplementary Information The online version contains supplementary material available at https://doi.org/10.1038/s41598-024-84037-4.

Correspondence and requests for materials should be addressed to C.A.G.

Reprints and permissions information is available at www.nature.com/reprints.

Publisher's note Springer Nature remains neutral with regard to jurisdictional claims in published maps and institutional affiliations.